Wiley Analytical Science

Forensic Applications of Rapid GC-MS: Seized Drug and Ignitable Liquid Screening

April 18th at 1:00pm EDT

There is a continued need across forensic science disciplines for the development of rapid screening methods that produce high-quality, specific results to address case backlogs and lengthy case analysis protocols. The need for new technologies, however, must be balanced with the time and manpower required to implement and validate such new techniques.

Watch this session during the WAS Virtual Conference:

Dr. Edward Sisco

Briana Capistran

Lakshmi Krishnan

Register Now

This talk is sponsored by Agilent

Received: 11 March 2021 | Revised: 7 June 2021 | Accepted: 8 June 2021

DOI: 10.1002/mas.21726

REVIEW ARTICLE

WILEY

UV-vis spectroscopy of gas-phase ions

František Tureček

Department of Chemistry, University of Washington, Seattle, Washington, USA

Correspondence
František Tureček, Department of Chemistry, University of Washington, Bagley Hall, Box 351700, Seattle, WA 98195-1700, USA.
Email: turecek@chem.washington.edu

Abstract

Photodissociation action spectroscopy has made a great progress in expanding investigations of gas-phase ion structures. This review deals with aspects of gas-phase ion electronic excitations that result in wavelength-dependent dissociation and light emission via fluorescence, chiefly covering the ultraviolet and visible regions of the spectrum. The principles are briefly outlined and a few examples of instrumentation are presented. The main thrust of the review is to collect and selectively present applications of UV-vis action spectroscopy to studies of stable gas-phase ion structures and combinations of spectroscopy with ion mobility, collision-induced dissociation, and ion–ion reactions leading to the generation of reactive intermediates and electronic energy transfer.

KEYWORDS

action spectroscopy, electronic excitations, ion fluorescence, ion mobility, ion protomers, reactive intermediates

1 | INTRODUCTION

The mass spectrum contains information which is encoded in a binary system of m/z values and ion intensities. This vector alone does not provide any other information regarding the ion chemical structure besides mass, charge, and, in case accurate mass data are obtained, a narrow range of plausible elemental compositions. Mass spectrometry often deals with this deficit by applying the process of spectra interpretation, which is based on generalized principles of ion reactivity. For example, the presence of two singly charged ions in the spectrum that differ by 15 m/z units is interpreted as pointing to the presence of a methyl group in the starting molecule (McLafferty & Turecek, 1993). This principle often holds, although there are known exceptions, one of those being the electron ionization spectrum of cyclohexane, which shows a loss of CH_3 even though this group is absent in the analyte molecule. The same limitations apply to multidimensional spectra (MS^n) obtained by activation and dissociation of mass-selected ions from the primary mass spectrum. In contrast to mass spectrometry, spectroscopic methods using frequency-dependent absorption of electromagnetic radiation rely on specific chromophores that can be assigned to particular functional groups or nuclei. This is the basis of absorption spectroscopies, such as UV-vis, infrared, NMR, and others. Mating spectroscopy to mass spectrometry can be expected to add an orthogonal dimension to ion structure elucidation. The well-known problem with this approach (Antoine & Dugourd, 2013; Baer & Dunbar, 2010; Forbes et al., 2009; Polfer & Dugourd, 2013) is that ion populations in the vacuum system of a mass spectrometer represent optically extremely thin samples, and so absorbance measurements, based on the difference between the incident and transmitted light intensity, are likely to be drowned by the incident light beam intensity fluctuations. There have been successful applications of direct measurements of ion spectra that relied on careful background suppression in emission (Allan et al., 1976, 1978; Maier, 1982, 1988, 1991) and fluorescence spectra (Maier & Thommen, 1981). Ion fluorescence measurements have recently enjoyed a renaissance, especially regarding larger biomolecular ions, as covered in Section 5 below. Ion spectroscopy in rare gas matrices has been applied successfully to obtain UV-vis absorption spectra of several small organic ions, for example, m- and p-$C_6H_4F_2^{+\bullet}$ and $C_6F_6^{+\bullet}$ (Bondybey

et al., 1980), and other ions (Batalov et al., 2006; Forney et al., 1989; Leutwyler et al., 1983). Absorption spectroscopy of matrix-isolated ions generated in the gas phase has been pioneered by Maier and coworkers. In their experimental setup (Leutwyler et al., 1983), ions were generated in the gas phase by electron ionization, mass-selected by a quadrupole filter, and deposited in a frozen neon matrix. UV-vis absorption spectra were obtained in a total-reflection waveguide fashion. In this way, absorption spectra of a number of small molecular ions have been obtained that showed vibrationally resolved states. However, the most fruitful approach to ion spectroscopy has combined light excitation with ion dissociation in what is called *action* or *consequence* spectroscopy (Polfer & Dugourd, 2013). This approach is based on ion photodissociation that was pioneered by several research groups in the 1970s (Dunbar, 1971) and 1980s (Hettich & Freiser, 1986), as recently reviewed (Gunzer et al., 2019). For example, in an early study, Dunbar used a xenon lamp as a light source to obtain a photodissociation spectrum of $CH_3Cl^{+\bullet}$ in the to 380–450 nm region that showed a broad band with an absorption maximum at 340 nm (Dunbar, 1971). Single-wavelength photodissociation of gas-phase ions in the visible and ultraviolet regions of the spectrum has become more widespread with the availability of compact lasers and now represents a complementary method for activation and dissociation of biomolecular ions (Brodbelt et al., 2020). Accordingly, this review is in part focused on recent developments of UV-vis action spectroscopy as applied to polyatomic ions related to biomolecules and transient intermediates of chemical reactions.

The scheme for UV-vis action spectroscopy (UVPD) relies on a single-photon excitation from the ground electronic state, S_0 for closed shell ions, D_0 for cation radicals, or higher spin states for transition metal complexes, depending on the ion ground-state spin multiplicity (Figure 1). The left-hand panel depicts the situation where a bound first excited state accessed by excitation overlaps with a dissociative higher excited state. In this case a nonadiabatic crossing to the dissociative state results in very fast dissociation, practically in a single vibration, from the excited state. A typical example of this type of excitation is photodissociation of aromatic iodides (Dzvonik et al., 1974). UV photon absorption promotes electron excitation of the $\pi \rightarrow \pi^*$ type within the aromatic ring, which is followed by a $\pi^* \rightarrow \sigma^*$ state crossing to the dissociative state, resulting in homolytic cleavage of the C–I bond and loss of iodine. The UV photon energy at wavelengths below 300 nm (>400 kJ mol^{-1}) is sufficient to break the C–I bond. A similar mechanism has been established for photodissociation of other types of organic molecules and ions,

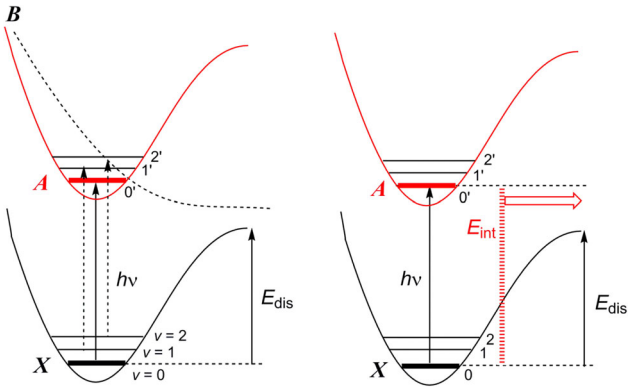

FIGURE 1 Excitation schemes in UV-vis action spectroscopy [Color figure can be viewed at wileyonlinelibrary.com]

such as hydrides, halides, and so on (Ashfold et al., 2010), as applied to iodotyrosine tagged peptide ions (Kirk et al., 2013).

For other types of chromophores, photon absorption leads to a bound excited state (Figure 1, right panel). In this case, the excited state undergoes a fast internal conversion to the vibrationally excited ground electronic state in which the excitation energy (E_{int}) is conserved and can promote dissociations occurring on the potential energy surface of the ground electronic state. This scheme has several implications regarding ion action spectroscopy. First of these is that to observe "action," the energy acquired by photoexcitation must exceed the thermodynamic threshold for the lowest energy dissociation. This can be a limitation for absorption in the visible region of the spectrum (400–700 nm) with photon energies in the range of 3.10–1.77 eV. In addition, for photodissociation to be observable, it must be sufficiently fast to occur on the time scale of the measurement, which can vary from microseconds to tens of milliseconds, depending on the type of instrument. The Figure 1 scheme presumes a resonant absorption of a single photon. However, in case of a strong chromophore and short excited-state lifetime, internal conversion of the electronic excited state can occur within a few hundreds picoseconds, and so the vibrationally hot ground-state ion can absorb a second photon from the same nanosecond-wide laser pulse. In this case the absorption band of the hot ion will be different from that of the initial state, but the absorption bands of hot ions are broad enough to ensure overlap with the laser wavelength. An example indicating a sequential two photon excitation is illustrated with the action spectrum of crystal violet ions (CV^+, Figure 2). The overall photodissociation spectrum shows bands with maxima at 560 and 290 nm that are very similar to those in the absorption spectrum of CV^+ in solution (Zollinger, 1987). The additional information obtainable from the action spectrum is that loss of two methyls from the CV dimethylamino groups apparently

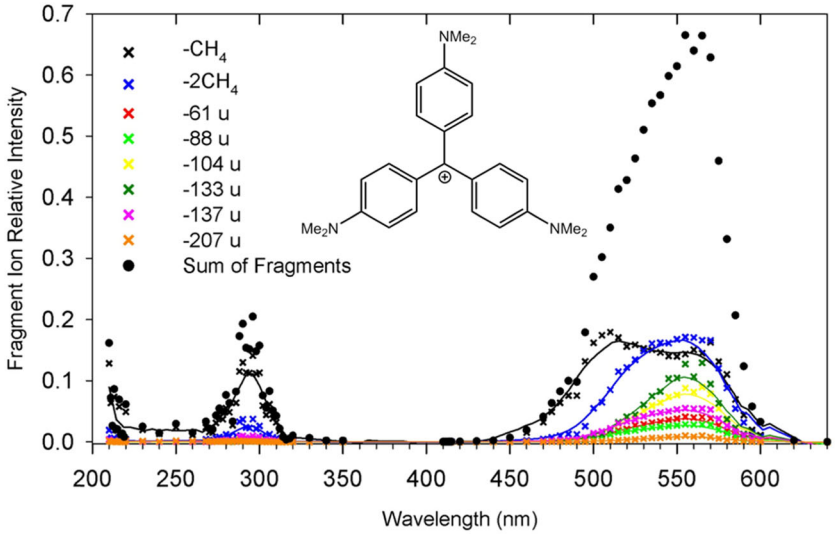

FIGURE 2 UVPD action spectrum of mass-selected crystal violet cation at *m/z* 372 [Color figure can be viewed at wileyonlinelibrary.com]

occurs at a lower photon energy than the loss of the first methyl, despite the latter having a lower-energy dissociation threshold. This effect can be attributed to a sequential absorption of two photons in the intense transition at 590 nm where excitation by the second photon drives consecutive dissociation of two methyl groups. Other examples of action spectra involving two- or three-photon excitation of strongly absorbing dye ions have been reported (Daly et al., 2014; Forbes & Jockusch, 2011; Wellman & Jockusch, 2015). Multiphoton excitation schemes in the UV-vis region are not very common, although multiphoton action spectra of several cyanine dyes absorbing at the edge of the visible and near IR region (700–800 nm) have been reported recently (Herve et al., 2019).

An important component of UV-vis action spectroscopy is spectra interpretation with the help of quantum chemistry calculations. These greatly benefit from the development of time-dependent density functional theory (TD-DFT) calculations (Furche & Ahlrichs, 2002) providing vertical excitation energies and oscillator strength for a number of excited states, optimized excited-state geometries, and molecular orbital analysis of electronic transitions. The selection of the density functional from the large and still growing number of available hybrid schemes is often important for achieving acceptable match between the calculated absorption spectrum and the experimental action spectrum. This has been addressed in several studies (Caricato et al., 2010; Gonzalez et al., 2012; Hait & Head-Gordon, 2021; Laurent & Jacquemin, 2013; Leang et al., 2012; Peach et al., 2008; Riffet et al., 2014; Silva-Junior et al., 2008; Sonk & Schlegel, 2011; Tureček, 2015). For smaller molecular systems, currently limited to under ca. 100 atoms but bound to increase with the advances in computer technology, it has become manageable to use correlated ab initio methods based on equation of motion, configuration interaction, or other theoretical approaches to study excited electronic states. An equally important development, helping the interpretation of UV-vis action spectra of thermal ions, has been programs allowing calculations of vibronic transitions from multiple vibrational states of the ground-state ions (Barbatti et al., 2014). Applications of these methods have furnished theoretical absorption spectra that provided improved match with UV-vis action spectra.

2 | INSTRUMENTATION

A successful photodissociation experiment must ensure efficient overlap of the ion population with the light source, which invariantly is a tunable pulsed laser. This can be achieved on ion beam instruments, but the most commonly UVPD has been performed with trapped ions. To illustrate UVPD on a beam instrument, the large-scale University of Aarhus tandem mass spectrometer (Støchkel et al., 2011; Wyer & Brøndsted Nielsen, 2012) is shown in Figure 3. Ions are produced by electrospray ionization in a source which is mounted on a high-voltage (±50 kV) platform. Ions are stored in a 14-pole ion trap, accelerated by dropping to the ground potential, and mass-selected by a large-radius inhomogeneous magnetic sector. The mass-selected and focused ion beam is sent down a long field-free region where the ions are intercepted by a laser beam aligned with the ion beam. UVPD products are analyzed according to their kinetic energies by a hemispherical electrostatic analyzer. A specific feature of the Aarhus instrument is that it allows one to study ion photodissociations occurring on a low-microsecond time scale. At high kinetic energies, ions are prone to collision-induced dissociation (CID) even at low pressures of residual gas, and careful corrections must be made to distinguish CID and UVPD products.

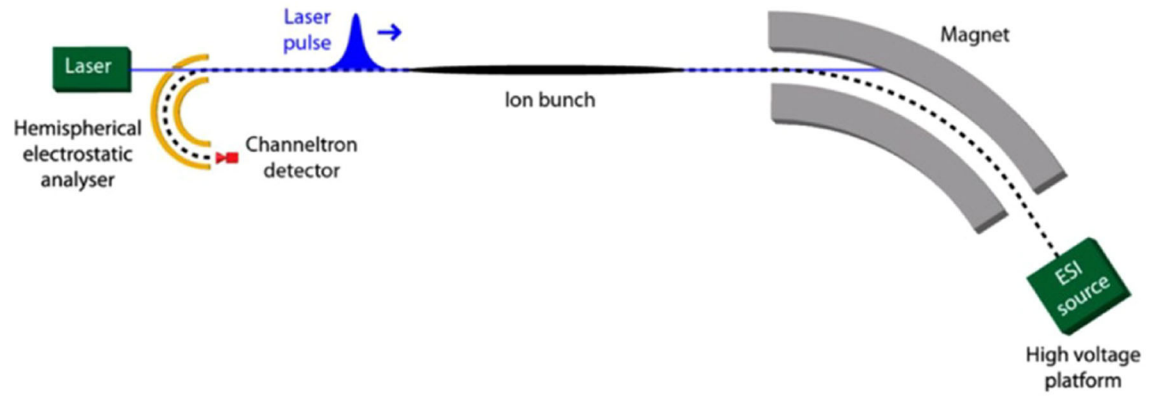

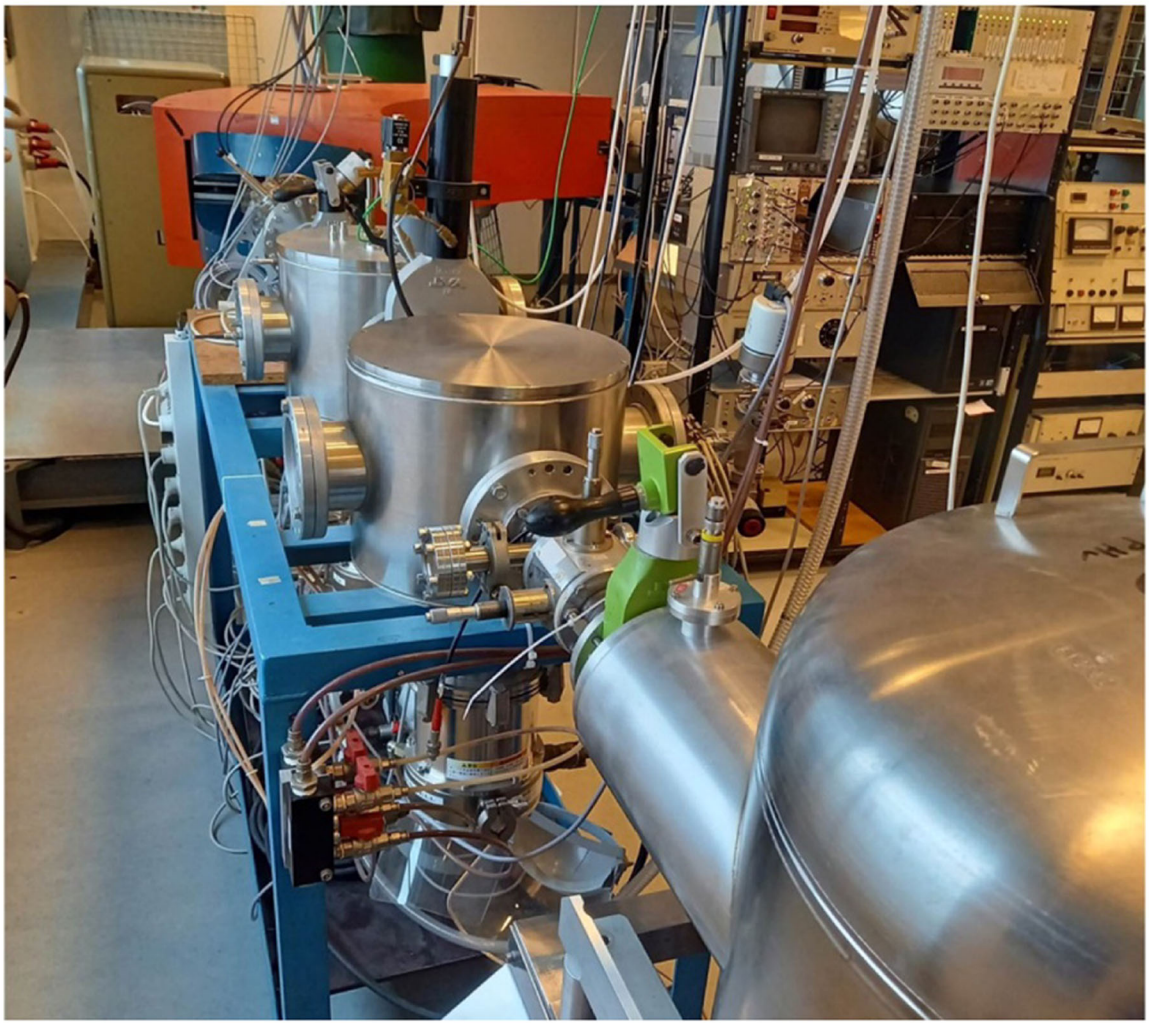

FIGURE 3 Top: Scheme of the Aarhus tandem instrument. Bottom: picture of the photodissociation field-free region containing collision cells [Color figure can be viewed at wileyonlinelibrary.com]

Beam instruments were used in the early development of ion photofragmentation spectroscopy which is a term that preceded action spectroscopy. A common feature of these instruments was that they used the turning point of ion trajectories in a reflectron time-of-flight mass analyzer as the locus for photodissociation (Cornett et al., 1992; Husband et al., 1999). The principle is sketched in Figure 4, omitting a number of technical details.

Ions, accelerated from the ion source, are selected by their arrival time when passing a pulsed electrostatic gate, while ions of other arrival times are deflected. The selected ion packet is focused and decelerated in the reflectron lens. The ion packet is intercepted by a pulsed

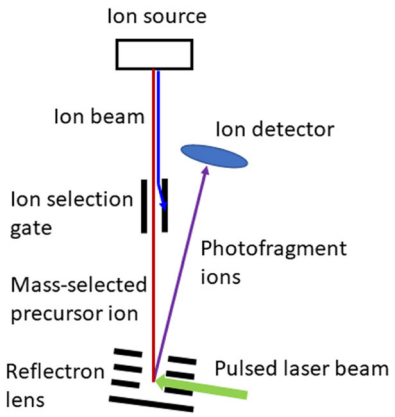

FIGURE 4 Scheme reflectron-time-of-flight instrument for ion photodissociation [Color figure can be viewed at wileyonlinelibrary.com]

laser beam at the turning point where the ions are slowed down to a low velocity and spatially compressed to increase the absorber optical density. Photofragment ions formed in the turning point region are reaccelerated by the reflectron potential gradient and separated by their flight time to provide the mass spectrum. The original instrument of Duncan et al. used laser ablation and pulse discharge ionization to generate metal ions that were reacted with cold molecules from supersonic expansion in a molecular beam (Cornett et al., 1992). The more recent version by Metz et al. can be outfitted with an electrospray ion source for making a wider range of ions (Johnston, Gentry, et al., 2018). In addition, this second generation instrument has a cold ion trap for the generation of ion–molecule complexes, and a second laser intercept region that allows photofragment imaging to determine the fragment velocity distribution and kinetic energy release in photodissociation.

Most of UVPD action spectroscopy measurements have so far been performed with trapped ions. A less typical ion trap system is represented by the electrostatic ion storage ring (ELISA) designed and built at University of Aarhus (Andersen et al., 2002). Ions are produced by electrospray, mass-selected, and formed into a bunch, which is accelerated to a 22 keV kinetic energy and stored in a large electrostatic ring. Laser photodissociation of the trapped ions forms fragments of proportionally lower kinetic energies, so that charged fragments do not pass the next round of the ring or can be gated out electrostatically. In contrast, neutral photofragments of keV kinetic energies formed along the straight path of the ring pass the gate and are detected in a side arm. This instrument has been used for ion spectroscopy studies of several polyatomic ions, such as protonated quinolones (Klaerke et al., 2011), flavins (Lincke et al., 2018), and retinal derivatives (Musbat et al., 2018).

The more typical experimental setup consists of a quadrupole ion trap mass spectrometer, linear or 3D, to perform ion formation, selection by mass, and storage for photodissociation (Nolting et al., 2004). In its simplest rendition, linear and 3D ion traps have been used to provide analysis of photofragment ions by mass-instability ejection or in combination with tandem mass spectrometry (Dang, Korn, et al., 2019). To obtain vibrationally resolved spectra, there has been much interest in carrying out photodissociation of trapped ions that were radiatively cooled to low temperatures (Alata et al., 2013; Bieske & Dopfer, 2000; Choi et al., 2009; Wang & Wang, 2008). The performance of a single ion trap, when used for all ion manipulations, has been shown to be adversely affected by the thermal contraction of the trap electrodes at low temperatures (17 K), which resulted in mass-scale shifts. This effect has been shown to be more significant at higher m/z values and its correction required a careful recalibration of the mass scale (Tesler et al., 2018). Hence, low-temperature UVPD measurements have been performed in a tandem set up, whereby the cold ion trap was used to store the ions to be photodissociated, while mass analysis of photofragment ions was accomplished after ejecting all ions to be accelerated and separated by a time-of-flight mass analyzer.

The difference between the action spectra of room-temperature and cold ions can be illustrated with protonated uracil. The room-temperature ion showed two broad absorption bands for the excitation from the ground-state singlet state (S_0) to the S_1 and S_2 excited states with maxima at 300 and 255 nm, respectively (Pedersen et al., 2014). Transitions between vibrational states, $0 \rightarrow 0'$, $1 \rightarrow 0'$, $0 \rightarrow 1'$, and so on, were not resolved under these conditions. The action spectrum of cold ions obtained at 20–50 K showed the same bands at 268–320 nm and 230–258 nm that were vibrationally resolved (Berdakin et al., 2014). The resolution and assignment of the vibrational bands allowed the authors to identify different ion tautomers. For example, the bands for protonated uracil were identified as belonging to the O-2, O-4 (230–258 nm), and N-3, O-4 (268–320 nm) tautomers formed by electrospray. In contrast, protonated cytosine and thymine were found to be formed as single tautomers (Berdakin et al., 2014).

UV photodissociation of cold ions is the basis of two other techniques. One uses combined fixed-wavelength UV photodissociation and scanned IR excitation that provides information on ion vibrational modes. In this approach (dip spectroscopy), a vibrationally resolved transition in the ion UV spectrum is selectively excited, leading to photodissociation. This requires a suitable chromophore, often an intense $\pi \rightarrow \pi^*$ transition in an aromatic group. The precursor ion is simultaneously

irradiated by a tunable infrared laser, whereby a $0 \rightarrow 1$ excitation of a resonant vibrational mode depopulates the $v = 0$ state, resulting in a diminished photodissociation yield (a dip) (Rizzo et al., 2009). The instrumentation and applications of UV-IR double-resonance spectroscopy have been reviewed (Bakels et al., 2019; Booth et al., 2016; Burke et al., 2015; Lemmens et al., 2020; Singh & Patwari, 2008; Svendsen et al., 2010) and will not be covered in this article.

The other technique uses noncovalent adducts of cold analyte ions with inert gas atoms (Ne, Ar) or molecules (D_2, N_2) admitted to the cold ion trap. This technique has found its main applications in single-photon infrared action spectroscopy (Bieske & Dopfer, 2000), but it has also been used for photodissociation in the UV-vis region (Jasik et al., 2015; Navratil et al., 2017; Srnec et al., 2018).

A UV-UV hole-burning experiment for gas-phase ions has been reported (Feraud et al., 2014). In this two-laser experimental setup, a population of ions is irradiated by the first laser in a cold ion trap, ejected, accelerated to keV kinetic energies, and sent to a time-of-flight analyzer, where the ions are intercepted by the second (probe) laser. Photodissociation products formed in this region are detected as neutral fragments of keV kinetic energies while ion products are stopped by an electrostatic gate. Hole burning is observed as depopulation of ions due to irradiation in the cold trap.

There has been a number of stable, polyatomic, even-electron gas-phase cations and anions generated by electrospray ionization for which UV-vis action spectra have been measured and interpreted. Among anions, firefly luciferin (Støchkel et al., 2011), nitrophenolates (Dodson et al., 2018; Pedersen & Nielsen, 2018), and DNA anions (Daly et al., 2019; Marlton et al., 2019) have been the most popular targets. The range of cations studied by UV-vis has been much wider, ranging from simple metal complexes to biomolecular ions.

3 | METAL COMPLEXES

The groups of Brucat and Duncan have reported a number of studies in which vibrationally resolved UV action spectra of weakly bound metal complexes were used to glean binding energies and vibrational structure of excited electronic states. These primarily involved atomic complexes of singly charged ions, such as $[Co^+Ar]$ and $[Co^+Kr]$ (Lessen & Brucat, 1989) and $[V^+Ar]$ and $[V^+Kr]$ (Lessen & Brucat, 1989), absorbing in the visible region above 600 nm, and $[Mg^+Ar]$ and $[Ca^+Ar]$ absorbing in the UV region (Duncan, 1997). Metz and coworkers have studied a range of complexes of singly charged transition metal ions with small molecules, such as $[Ni^+OH]$, $[Ni^+(H_2O)]$ (Daluz et al., 2012; Thompson et al., 2000), $[Ni^+(H_2O)_{4\text{-}7}]$ (Thompson et al., 2000), $[Au^+(C_2H_4)]$ and $[Pt^+(C_2H_4)]$ (Stringer et al., 2004), $[V^+(OCO)]$ (Citir et al., 2006), $[TiO^+(CO_2)]$ (Perera & Metz, 2009), $[Co^+(H_2O)]$ (Kocak et al., 2013), $[Mn^+(H_2O)]$ (Pearson et al., 2014), $[Cr^+(NH_3)]$ (Ashraf et al., 2018), and MnO^+ (Johnston, Gentry, et al., 2018). A VUV photoionization study of Au^+ reactions with ethylene and acetylene has been reported (Metz et al., 2019).

Among those, these authors used ion-molecule reactions of FeO^+ with methane to generate a jet-cooled aquo carbene complex, $[H_2C{=}Fe{-}OH_2]^+$. An isomeric insertion intermediate, $[HO{-}Fe{-}CH_3]^+$(Aguirre et al., 2002) was generated by an ion–molecule reaction with methanol. Both these ions have been considered as thermodynamically stable high-spin intermediates of the important Fe-catalyzed oxidation of methane to methanol (Crabtree, 1995). $[H_2C{=}Fe{-}OH_2]^+$ was characterized by the vibrationally resolved band having an onset at 730 nm which indicated a photodissociation threshold of 1.7 eV. The spectrum of $[HO{-}Fe{-}CH_3]^+$ was distinctly different, showing a well resolved band with an onset at 325 nm with three vibrational progressions due to the Fe–C (ν_{11}) and Fe–O (ν_8) stretching modes, and an O–Fe–C bending mode (ν_{14}) that were assigned using the spectrum of $[HO{-}Fe{-}CD_3]^+$ (Aguirre et al., 2002; Metz, 2004). Action spectra of complexes of transition metal dications with small molecules have been reported for $[Co^+(H_2O)_{4\text{-}7}]$ (Faherty et al., 2001), $[Co^{2+}(CH_3OH)_{4\text{-}7}]$ (Thompson et al., 2005), $[Co^{2+}(CH_3CN)_n(H2O)_m]$, and $[Ni^{2+}(CH_3CN)_n(H2O)_m]$ (Metz, 2004; Perera et al., 2011).

The photodissociation action spectrum of Au_2^+, cooled to 150 K and acquired in the 300–700 nm range, has been recently reported (Foerstel et al., 2020). Theoretical interpretation of transitions in the vibrationally resolved 310–330 nm band in the spectrum required high-level calculations at the multireference CASSF-MRCI level including relativistic treatment of spin-orbit coupling. No less than seven electronic states have been considered in the spectra interpretation. The authors pointed out that DFT calculations were inadequate for this electronically complex system. Chromium dimer ions, Cr_2^+have been studied by cold-ion spectroscopy at 7–10 K (Egashira & Terasaki, 2015). The ions were found to be extremely susceptible to ion–molecule reactions with residual O_2 that were prevented by oxygen cryotrapping. Both absorption and action spectra of Cr_2^+ were obtained and compared, giving an absorption maximum at 2.21 eV (560 nm).

The electronic properties of the prototypical CuO^+ ion have been studied using a complex with CH_3CN (Srnec et al., 2018). The choice of the complex was dictated by the high reactivity of naked CuO^+ which did not survive passage through the high pressure region of the

electrospray ion source. The cold $[CuO^+(CH_3CN)]$ complex at 5 K was tagged with Ne, and action spectra were obtained in the visible and near-IR wavelength regions. The spectrum showed band progressions in the 500–600 nm region due to multiple transitions from the ^3A ground state to triplet excited electronic states.

UV-vis action spectroscopy has been used to identify products of gas-phase addition of water to 2,2′-bipyridine complexes of metal oxide ions (bpy)Met=O^+, (Met = Cu, Ni, Co), that were generated in the gas-phase by collision-induced dissociation of ternary nitrate complexes (Dang, Nguyen, et al., 2018). The mass-resolved action spectra allowed a distinction to be made between isomeric water complexes of (bpy)Cu=O^+ and (6-hydroxy-2,2′-bipyridine)Cu^+ (Figure 5). The water adducts to (bpy)Cu=O^+ were assigned to a mixture of singlet $[Cu(bpy)(OH)_2]^+$, in which the water molecule was split into two Cu-bound OH groups, and triplet $[Cu(bpy)(O)(OH_2)]^+$isomers. The substantially more stable $[Cu(6\text{-hydroxy-2,2′-bipyridine})(OH_2)]^+$isomer has been clearly distinguished not only by the absorption band maxima (Figure 5), but also by the major channel for photodissociative elimination of water. In contrast, the $[Cu(bpy)(OH)_2]^+$ complex underwent photochemical loss of OH, resulting in a near-UV splitting of the coordinated water molecule. The mass-resolved photodissociation channels added another degree of specificity to isomer distinction by UV-vis action spectroscopy.

Nitrogen tagging of cold ions has been used to obtain action spectra of metal tris-(2,2′-bipyridine) complexes of Fe, Os (Xu et al., 2017), and Ru (Xu et al., 2016a), following a broader survey study of photodissociation of thermal tris-bpy complexes of Mn, Fe, Co, Ni, Cu, and Zn dications (Xu et al., 2016b). The tris-(2,2′-bipyridine)ruthenium(III) ion has been the subject of earlier studies that used thermal ions (Kirketerp & Nielsen, 2010; Stockett & Broendsted Nielsen, 2015). Larger metal-coordinated ions have been studied by action spectroscopy, as reported for heme nitrosyl cations (Wyer & Brøndsted Nielsen, 2012), and dibenzo-18-crown-6-ether complexes of alkali metal cations (Choi et al., 2009).

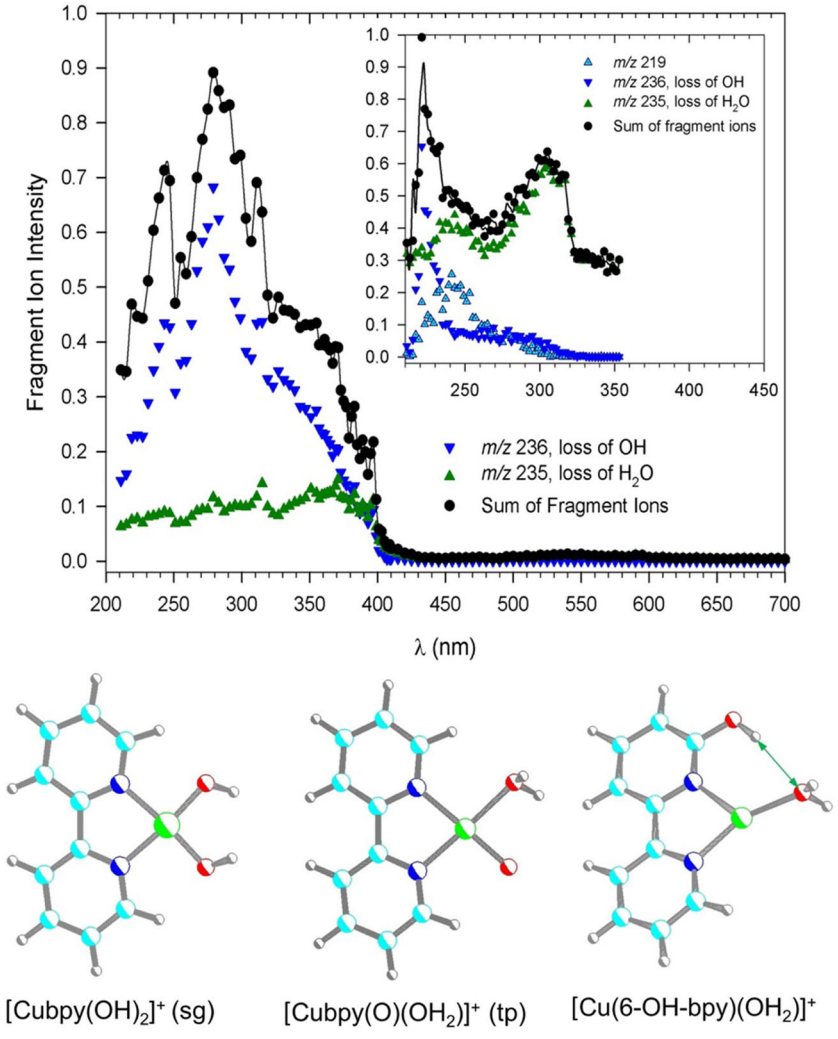

FIGURE 5 UV-vis action spectra of $[Cu(bpy)(O_2H_2)]^+$ isomers and $[Cu(3\text{-OH-bpy})(H_2O)]^+$ complex (inset) (Dang, Shaffer, et al., 2018). The color coding in the structure drawings is as follows: C, cyan; Cu, green; H, gray; N, blue; O, red [Color figure can be viewed at wileyonlinelibrary.com]

4 | MISCELLANEOUS ORGANIC IONS

Action spectra of a number of polyatomic gas-phase ions have been reported that naturally included ions possessing strong chromophores with aromatic and heteroaromatic systems (Soorkia et al., 2020). UV-vis action spectra have been reported for protonated tryptophan (Nolting et al., 2004) and dipeptide Leu-Trp ions (Nolting et al., 2006), indole (Alata et al., 2013), *N*-methylpyridinium (Hansen, Kirk, Blanksby & O'Hair, & Trevitt, 2013), nicotinamide (Matthews & Dessent, 2016), quinoline and isoquinoline (Hansen et al., 2015), and rhodamine 575 (Daly, Kulesza, Knight, et al., 2015). Spectra of cold rhodamine ions (Rhodamine 123, 110, and its Ag salt) have been obtained at 3 K using the helium-tagging technique (Jasik et al., 2015), and the effects of ion temperature and tagging have been investigated in another study (Navratil et al., 2017). Among other aromatic ions, action spectra have been reported for the conjugated tripyrrole prodigiosin (Drink et al., 2015), quinazoline (Marlton et al., 2020), haloanilinium ions (Hansen, Kirk, Blanksby & O'Hair, & Trevitt, 2013), tautomers of protonated aminonaphthalenes (Noble et al., 2018), azobenzenes (Feraud et al., 2016), and vinylheptafulvene derivatives (Elm et al., 2015). Cold corannulene cations embedded in helium nanodroplets have been studied by action spectroscopy (Gatchell et al., 2019). Spectra of host–guest complexes of protonated aniline with crown ethers have been reported (Inokuchi et al., 2015). A salient feature of UV-vis action spectra was their ability to distinguish protomeric ion structures that often showed distinct absorption bands. This has provided a new tool to studies of ion structure in addition to the more traditional multiphoton infrared action spectroscopy (Eyler, 2009; Polfer, 2011).

This feature of UV-vis action spectra is illustrated with protonated lumiflavin ions that can exist as N1 or O2 protomers (Mueller & Dopfer, 2020) (Scheme 1). Protonation of lumiflavin in solution has a large effect on the absorption spectrum where the S_1 band maximum shifts from 441 nm in the neutral form to 394 nm in the protonated form. The 420–500 nm band in the action spectrum of the cold (20 K) ion showed a vibronic structure that indicated the presence of the lower-energy O2 isomer ($HLF(O2)^+$), but also the N1 isomer ($HLF(N1)^+$ that was detected for the first time. The authors pointed out differences between the action spectra of cold naked cations and the absorption and fluorescence spectrum of neutral lumiflavin measured in superfluid helium nanodroplets (Vdovin et al., 2013). The photodissociation spectrum of protonated lumichrome has also been reported (Sheldrick et al., 2018).

A related group of studies included protonated nucleobases and nucleosides, as first reported for adenine

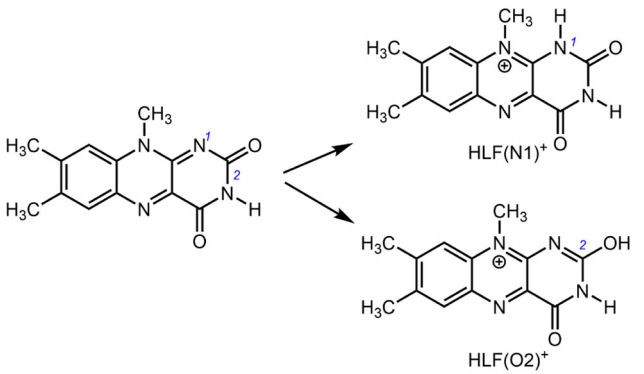

SCHEME 1 Protonation of lumiflavin and N1 and O2 ion tautomers

(Cheong et al., 2011; Marian et al., 2005; Nolting & Weinkauf, 2007), and then for adenosine (Pedersen et al., 2013), uracil and thymine (Pedersen et al., 2014), other nucleobases (Berdakin et al., 2014), and base-pair homodimers (Feraud et al., 2015).

At the high-mass end of action spectroscopy measurements, dye-loaded silicon oxide nanoparticles have been reported to absorb at 600 nm when irradiated in an ion trap. These experiments used a cold ion trap, and light absorption was monitored by desorption of N_2 molecules adhering to the cold nanoparticle ion surface (Hoffmann et al., 2020).

5 | ACTION SPECTROSCOPY IN COMBINATION WITH ION-MOBILITY

UVPD action spectroscopy is amenable to being coupled to other tandem mass spectrometry methods involving special techniques for ion generation and separation. On-the-fly ion separation before and after UVPD has been realized by Bieske at al. in a specially built instrument involving ion mobility drift regions (Adamson et al., 2013, 2014). Scheme 2 shows a simplified sketch of the instrument, incorporating two curved drift regions for ion mobility separation (IMS) of precursor and photo-product ions. In one mode of operation, a packet of precursor ions selected by the first ion-mobility drift region are irradiated by a transverse light beam from a tunable laser in the region between the first and second IMS. The products, which often are photoisomers, together with the initial ion population are separated by the second IMS, mass analyzed by a quadrupole mass filter, and detected.

The instrument has chiefly been used to study photoisomerization of carbocyanines dyes such as merocyanine-spiropyran (Markworth et al., 2015), but also other interesting model ionic systems such as *E* and *Z*-azobis(2-imidazole) (Bull et al., 2017), retinal derivatives (Coughlan et al., 2014, 2016), and a $C_4H_3^+$ ion (Catani et al., 2017).

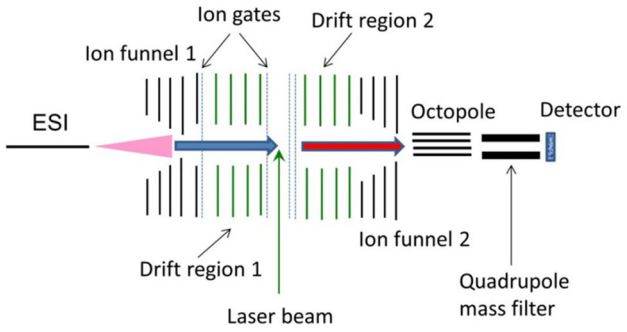

SCHEME 2 Combination of UV-vis action spectroscopy with ion mobility. Adapted from Bull et al. (2017) [Color figure can be viewed at wileyonlinelibrary.com]

Other studies by the same group included prototropic isomerization of *p*-coumaric acid anions (Bull et al., 2019), and flavin mono- and dianions (Bull et al., 2018). In a comprehensive study of multiple ion isomers (Bull et al., 2019), the authors used ion mobility to resolve *p*-coumaric (4-hydroxycinnamic) carboxylate and phenolate anions as E, Z-geometrical isomers produced by electrospray and collisional activation in the ion funnel (Scheme 3). Irradiation in the 300–380 nm region of the arrival-time selected carboxylate E-anion resulted in isomerization to the more stable phenolate anion that has been resolved by ion mobility in the second drift region. The phenolate anion showed a distinct absorption maximum at 430 nm that was outside the wavelength region used for photoisomerization. An oxo-protomer has been identified as a minor product of photoisomerization. In contrast, irradiation of the Z-carboxylate anion with a maximum at 320 nm chiefly resulted in electron photodetachment.

A recent modification of a Sciex Qtrap 5500 tandem mass spectrometer has been reported. The mass spectrometer was furnished with a tunable laser irradiating mass-selected ions that were stored in the Q3 linear ion trap. The authors utilized a front-end differential mobility region to separate quinoline and isoquinoline ions (Matthews & Dessent, 2016). UV-vis action spectra obtained on this instrument were shown to be comparable to the spectra obtained previously (Hansen et al., 2015). The combination of ion mobility and UV-vis action spectroscopy has also been applied to distinguish protonation isomers of quinazoline (Marlton et al., 2020).

6 | UV-VIS ACTION SPECTROSCOPY OF CATION RADICALS AND TRANSIENT INTERMEDIATES

The multistage capabilities of an ion trap have been conducive to experimental designs for the generation of polyatomic reactive ion species to be studied by UV-vis action spectroscopy. For example, the combination of tandem CID with UV-vis action spectroscopy (CID-UVPD-MS^3) has been used to generate and study several cation radicals related to nucleobases. Cation radicals of cytosine (Lesslie et al., 2017), guanine, 9-methyl guanine, and 2′-deoxyguanosine (Dang, Korn, et al., 2019), adenine, and 9-methyladenine (Huang, Dang, et al., 2020) have been generated by the technique developed by O'Hair and coworkers (Wee et al., 2005). This consists in producing by electrospray ionization a doubly charged ternary complex of the neutral nucleobase with a transition metal (typically Cu^{2+}) and an auxiliary polydentate ligand, such as 2:2′,6′:2″-terpyridine (Scheme 4).

CID of the mass-selected complex results in intramolecular electron transfer, ionizing the nucleobase and separating the singly charged product ions. The UV-vis action spectra of cation radicals of adenine, guanine, their methyl homologues, as well as those of cytosine have been interpreted as belonging to ground doublet states of canonical structures with bond connectivities analogous to those in the neutral nucleobases. The adenine, 9-methyladenine, guanine, 9-methylguanine and riboguanosine cation radicals showed weak absorption

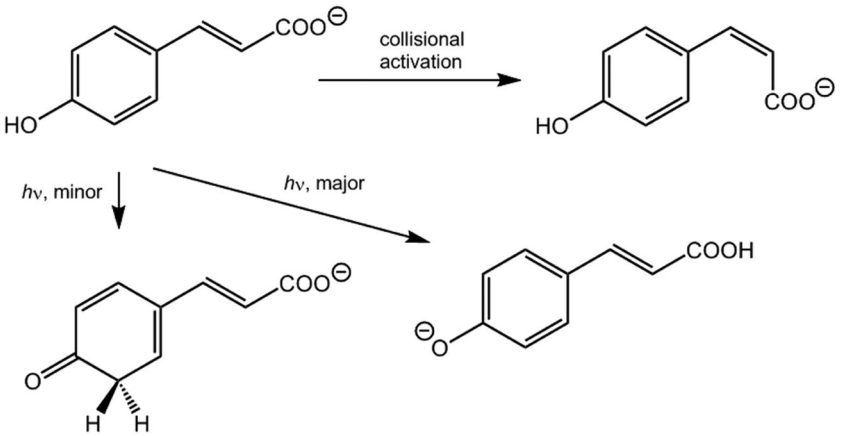

SCHEME 3 Thermal and photochemical isomerization of *p*-coumarate anions

bands in the visible region of the spectrum, typically between 500 and 600 nm that have been assigned to $\pi_z \rightarrow \pi_z$ (SOMO) inner electron excitations within the β-electron manifold. Transitions to the first excited states (A) have been calculated to be dipole disallowed and did not give rise to detectable absorption bands. These features, both the absorption wavelength and type of electron excitation to low excited states, distinguish the cation radicals from closed-shell nucleobase ions that do not absorb above 300 nm (Berdakin et al., 2014; Cheong et al., 2011; Feraud et al., 2015; Marian et al., 2005; Nolting & Weinkauf, 2007; Pedersen et al., 2013; Pedersen et al., 2014), and whose excitations are of the $\pi_z \rightarrow \pi_z^*$ type. In addition to natural nucleobases, the Scheme 4 reaction sequence has also been used to generate cation radicals of synthetic, so-called hachimoji nucleobases (Hoshika et al., 2019; Hutter & Benner, 2003) containing modified ring systems or substituents (Figure 6).

The cation radicals of B, P, and Z hachimoji nucleobases displayed UV-vis action spectra that indicated canonical structures corresponding with those of the neutral molecules. For example, the spectrum of hachimoji B showed very similar bands ($\lambda_{max} = 215$, 263, 330, and 355 nm with a shoulder at 400 nm) to those in the spectrum of guanine cation radical (Huang & Tureček, 2020, 2021). The longest detected wavelength band extending to the visible region was due to a $\pi_z \rightarrow \pi_z$ excitation to the third (C) excited state while excitations to the A and B states at 620 and 494 nm, respectively, were of the dipole-disallowed $\pi_{xy} \rightarrow \pi_z$ type. Interestingly, the six lowest excited states of $B^{+\bullet}$ in the 320–620 nm region all arose by excitations to the SOMO within the β-orbital manifold.

In addition to the formation of canonical nucleobase cation radicals, electron transfer in [Cu(terpy)nucleobase]$^{2+\bullet}$ complexes has been found to result in the formation of isomerized, Noncanonical cation radicals for thymine (Dang, Nguyen, et al., 2018) and hachimoji S base (Huang & Tureček, 2020) (Figure 7). The isomerization involved hydrogen atom migration from the methyl group onto a ring heteroatom.

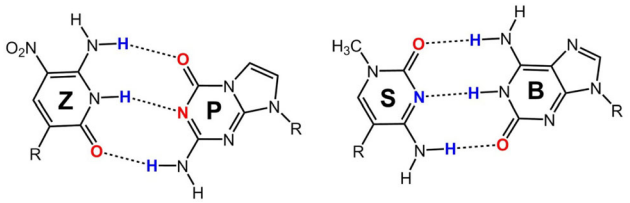

FIGURE 6 Base pairs of hachimoji nucleobases Z, P, S, and B [Color figure can be viewed at wileyonlinelibrary.com]

The action spectrum of the thymine ion showed distinctive absorption bands at 350 and 520 nm that were absent in the theoretical vibronic spectrum of the canonical isomer (Dang, Nguyen, et al., 2018). The 1-methylcytosine ion showed bands at 470 and 580 nm that distinguish it from the calculated vibronic spectrum of the canonical isomer. The major bands in the experimental spectra of both noncanonical thymine and 1-methylcytosine ions have been assigned to allowed $\pi_z \rightarrow \pi_z^*$ transitions from the SOMO to the virtual orbital space. In contrast, the low-energy electron excitations in the canonical thymine and methylcytosine cation radical isomers were all internal, involving transitions to SOMO within the β-electron manifold.

A noncanonical isomer of 9-methyladenine cation radical (Figure 7) was synthesized in the gas phase by CID-MS^2 of protonated 9-iodomethyladenine and characterized by UV-vis action spectroscopy (Huang et al., 2021). The spectrum showed a composite band at 360 and 400 nm from excitations to the A and B states that distinguished the ion from the canonical adenine cation radical that absorbed at 580 nm. According to the molecular-orbital representation of electron excitations (Figure 8), the lowest energy excitation in the canonical [9-methyladenine]$^{+\bullet}$ isomer occurred by a transition within the β-electron manifold. By contrast, the noncanonical isomer of 9-methyladenine cation radical showed excitations via $\pi_z \rightarrow \pi_z^*$ transitions from the SOMO and underlying molecular orbitals to the virtual orbital space.

Oxidation of Cu^{2+} (terpy) complexes has also been used to generate tyrosine-containing peptide cation

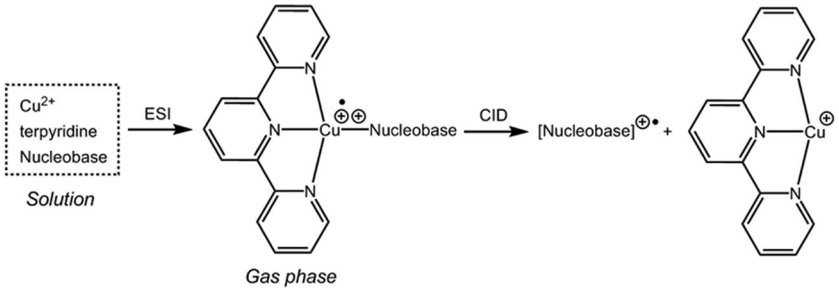

SCHEME 4 Formation of gas-phase nucleobase cation radicals

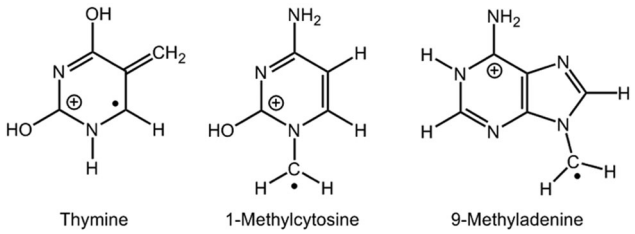

FIGURE 7 Noncanonical isomers of thymine, 1-methylcytosine, and 9-methyladenine cation radicals

radicals differing in their amino acid sequence, Tyr-Ala-Ala-Ala-Arg (YAAAR) and Ala-Ala-Ala-Tyr-Arg (AAAYR). These have been shown by UV-vis action spectroscopy to generate different types of peptide cation radicals (Viglino et al., 2016). $[YAAAR]^{+\bullet}$ was identified as an arginine-protonated tyrosyl O-radical which showed bands at 260, 300, and 360 nm in the UV-vis action spectrum, matching the absorption bands from TD-DFT calculations (Figure 9). Contrasting this, the action spectrum of $[AAAYR]^{+\bullet}$ showed multiple poorly

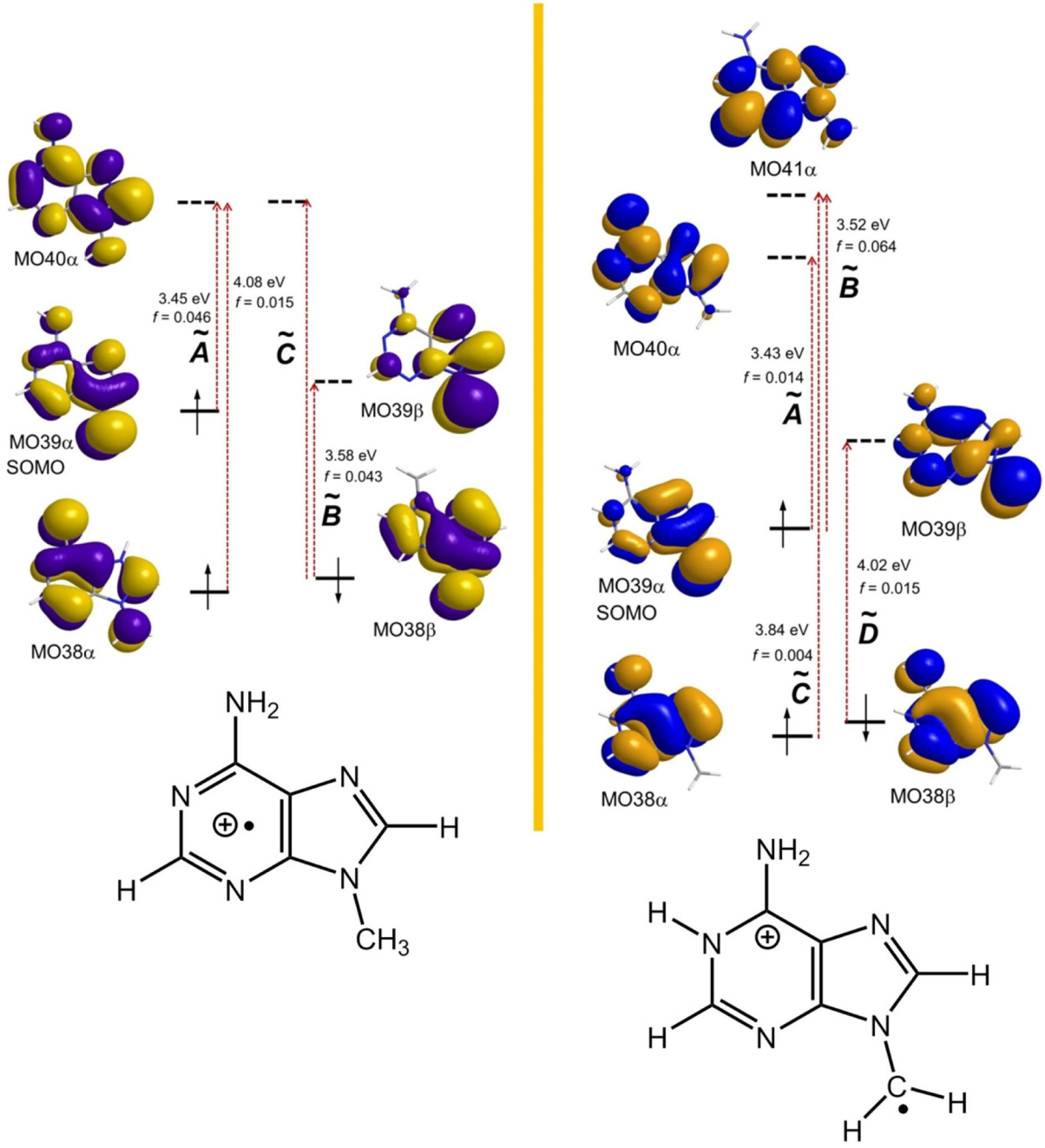

FIGURE 8 Molecular-orbital representation of electron excitations in canonical (left panel) and distonic (right panel) isomers of 9-methyladenine cation radical [Color figure can be viewed at wileyonlinelibrary.com]

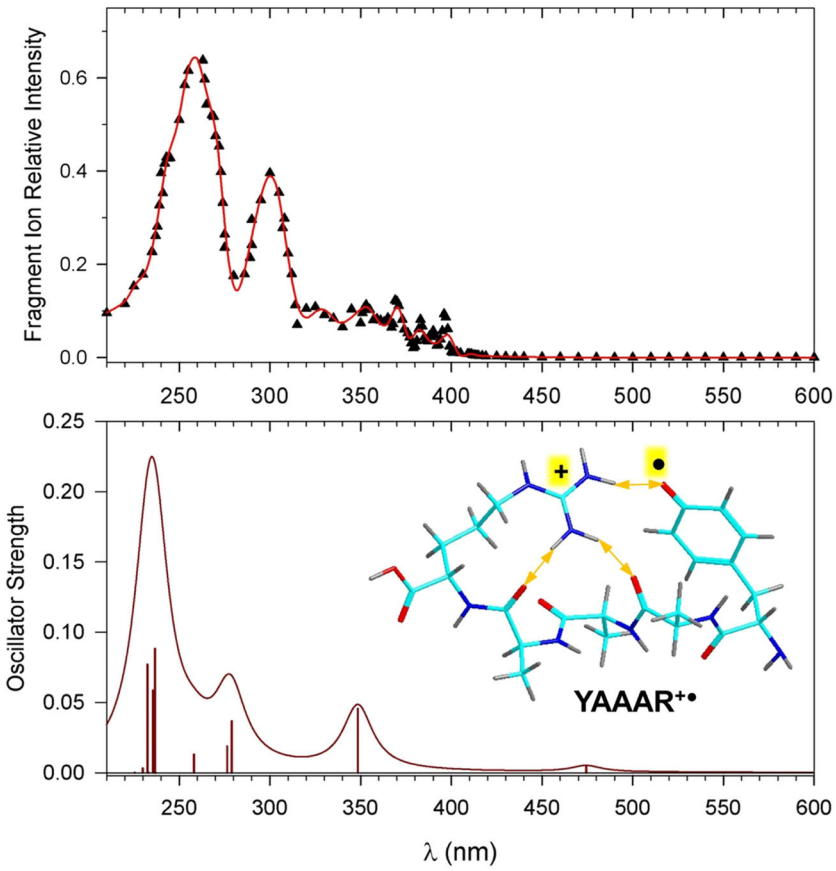

FIGURE 9 Top: UV-vis action spectrum of $YAAAR^{+\bullet}$ generated from a $[Cu(terpyYAAR]^{2+\bullet}$ complex. Bottom: ωB97X-D/6-31+G(d,p) TD-DFT absorption spectrum [Color figure can be viewed at wileyonlinelibrary.com]

resolved bands that according to TD-DFT calculations were assigned to a mixture of Arg-protonated isomers with radicals in the aromatic ring and C_α peptide positions.

In contrast to gas-phase oxidation leading to nucleobase and peptide cation radicals, reduction methods, based on electron transfer in gas-phase dication-anion reactions, have been used to generate a number of peptide, nucleoside, and oligonucleotide cation radicals and obtain their UV-vis action spectra. In a series of studies, peptide fragment ions of the *z*-type, $[HC^{\bullet}(R)CONH–]^+$, generated by electron transfer dissociation (Syka et al., 2004) of multiply protonated peptides, have been studied by UV-vis action spectroscopy (Imaoka et al., 2018; Nguyen et al., 2015, 2017; Pepin et al., 2017; Shaffer et al., 2015). For example, the $[^{\bullet}$Ala-Thr-Ala-Arg$]^+z$-ion, produced by ETD of $(AATAR + 2H)^{2+}$, has been shown to have the structure with a protonated arginine and the radical site at the terminal Ala C_α (Figure 10) (Nguyen et al., 2017).

The near-UV band with a maximum at 340–360 nm has turned out to be highly characteristic of peptide terminal C_α radicals. According to molecular orbital analysis, it corresponds to an excitation to the doublet B state by an allowed $\pi_z \rightarrow \pi_z$ transition of a β-electron from a lower molecular orbital to the SOMO (Shaffer et al., 2015). In contrast, peptide cation radicals with the capto-dative $[–NH-C^{\bullet}(R)CONH–]^+$ chromophore absorb at shorter wavelengths (Pepin et al., 2017). This selectivity has allowed the authors to distinguish spontaneous isomerizations of z-type ions having terminal Asn, Asp, Gln, and Glu residues that have been found to facilitate intra- and inter-molecular hydrogen atom transfer, moving the radical site from the *N*-terminal C_α position to internal positions within the peptide backbone (Imaoka et al., 2018).

UV-vis action spectroscopy has also been used to characterize several DNA and RNA nucleotide cation radicals that have been generated by electron transfer in the gas phase (Tureček, 2021). Upon one-electron reduction of dications, DNA dinucleotides and RNA chimeras (Korn et al., 2017; Liu et al., 2018) have been found to undergo a conformational collapse accompanied by exoergic proton- or hydrogen-atom transfer between the adenine cation and radical-carrying rings (Korn et al., 2017), and between the cytosine radical and guanine cation (Liu et al., 2018). This kind of an isomerization was found to depend on the dinucleotide sequence, occurring in $(GC + 2H)^{+\bullet}$ but not in $(CG + 2H)^{+\bullet}$ or $(CC + 2H)^{+\bullet}$ (Liu et al., 2019). Analogous proton/hydrogen atom transfers were revealed by analyzing UV-vis action spectra of tetranucleotide cation radicals $(GATC + 2H)^{+\bullet}$, $(AGTC + 2H)^{+\bullet}$ (Huang, Liu, et al., 2020), and $(GATT + 2H)^{+\bullet}$ and $(AGTT + 2H)^{+\bullet}$ (Liu, Huang, et al., 2020). These isomerizations occurred spontaneously

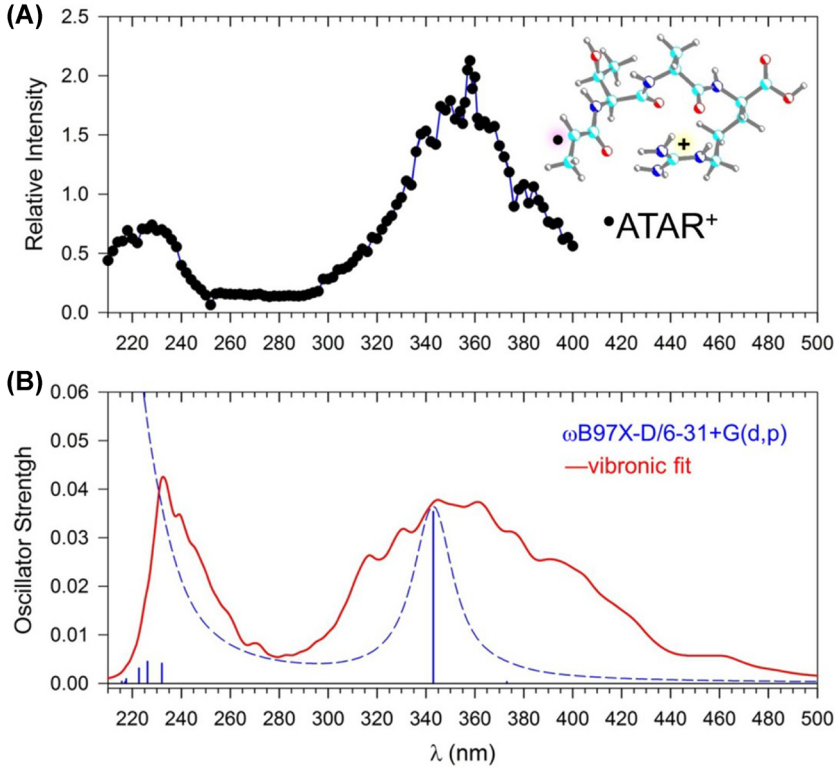

FIGURE 10 (A) UV-vis action spectrum of the z_4 ion from electron-transfer dissociation of $(AATAR+2H)^{2+}$ expressed as a sum of photofragment ion intensities. (B) Calculated TD-DFT transition energies and vibronic spectrum of a low-energy $^{\bullet}ATAR^{+}$ conformer at 310 K [Color figure can be viewed at wileyonlinelibrary.com]

upon one-electron reduction and were facilitated by very low transition state energies for nucleobase ion-radical interactions. RNA nucleoside radicals tagged at ribose with a fixed charge 6-(trimethylammonium)-1-hexaminecarbonyl appendage have been generated in the gas phase (Liu, Ma, Leonen, et al., 2021; Liu, Ma, Nováková, et al. 2021; Liu, Huang, et al., 2020) to be studied by UV-vis action spectroscopy. To obtain stable charge-tagged nucleoside radicals, the electron-transfer ion-ion reaction was carried out with noncovalent complexes of the respective doubly charged ions with a crown ether, which resulted in reduction and loss of the ligand while keeping the nucleoside cation radicals from dissociating. UV-vis action spectra of singly charged conjugates have also been reported in which the chromophore was a neutral nucleobase (Liu, Ma, Leonen, et al., 2021; Liu, Ma, Nováková, et al., 2021; Liu, Huang, et al., 2020). These have been the only measurements of UV-vis spectra of neutral nucleosides in the gas phase.

7 | VACUUM UV ACTION SPECTROSCOPY

A special application of action spectroscopy concerns excitations by photons in the 5–14 eV energy region corresponding to a 248–89 nm range of wavelengths. The high end of this wavelength range overlaps with standard UV where the excitations involve valence-bond electrons. At the lower end, both excitations from low-energy orbitals and higher excited states are sampled. Photons in this region are produced by synchrotron radiation and used to irradiate ions that are formed by electrospray and stored in an RF ion trap, also functioning as a mass analyzer, which is attached to the synchrotron (Milosavljevic et al., 2011, 2012, Rankovic et al., 2016). The spectra are plotted as energy-dependent cross sections of photofragmentation ion channels. This technique has been applied to a few ions, for example, perfluorooctanoate anion (Douix et al., 2018), protonated leucine-enkephalin (YGGFL) (Rankovic et al., 2015), and polysaccharides (Enjalbert et al., 2013). The peptide VUV action spectra showed a strong feature at ca. 6.9 eV (180 nm) that has been assigned to a peptide $\pi_2\pi_3^*$ electronic transition. Remarkably, the photodissociation mass spectra in the reported range of photon energies displayed fragment ions typical for peptide collision-induced dissociation.

8 | PHOTODISSOCIATION, FLUORESCENCE SPECTROSCOPY, AND INTRAMOLECULAR FORSTER RESONANT ENERGY TRANSFER (FRET) IN BIOMOLECULAR IONS

Detecting light emission from electronically excited gas-phase ions was one of the early applications of ion spectroscopy (Allan et al., 1976, 1978; Maier, 1988). With the advent of ion trapping techniques (Stockett et al., 2016), fluorescence measurements of gas-phase ions have been made

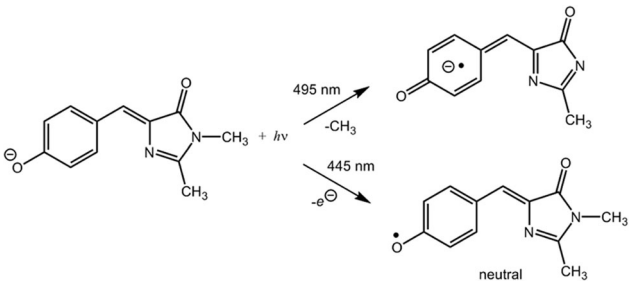

SCHEME 5 Photodisociation of green fluorescent protein chromophore anions

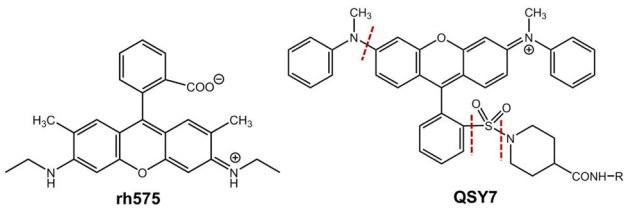

SCHEME 6 Chromophore tags used for a study of FRET effects in gas phase peptide ions. Broken lines indicate bond dissociations in the receptor that were used to study FRET. FRET, Förster resonance energy transfer

possible for strong chromophores in combination with action spectroscopy. The light-absorbing chromophore of the green fluorescent protein (GFP) has been studied in its anion form ($HBDI^-$) in the gas phase (Forbes et al., 2009, 2011). Irradiation of the anion was found to result in two major competitive processes which were loss of a methyl at 495 nm and electron detachment at 445 nm (Scheme 5). Consistent with solution studies, the anion showed no detectable fluorescence, indicating very rapid deactivation of the excited states by internal conversion. More recently, Fielding et al. studied the energetics of electron photodetachment from $HBDI^-$ and its several analogues (Bochenkova et al., 2017; McLaughlin et al., 2017; Mooney et al., 2012). $HBDI^-$ was found to have an adiabatic electron detachment threshold of 2.73 eV, representing the electron binding energy of the S_0 state. The photodetachment threshold was assigned to the $S_0 \rightarrow D_0$ electron excitation (Bochenkova et al., 2017). The molecular geometry of $HBDI^-$ with respect to the E or Z configuration at the exocyclic double bond has been studied by cold-ion spectroscopy of an $[HBDI^-{\bullet}N_2]$ adduct (Zagorec-Marks et al., 2019). The assignment was primarily based on an infrared action spectrum, but the vibrational profile of the absorption band at 476 nm was also consistent with the assigned Z geometry of the ion. UVPD spectra were also reported for untagged $HBDI^-$ that showed a ca. 10 nm blue shift of the main band as temperature was varied from 300 to 30 K. A 5-nm red shift was found due to the presence of the N_2 tag.

Fluorescence and photodissociation were compared in a study of gas-phase fluorescein (Yao & Jockusch, 2013) and rhodamine 110 cations. Both processes showed the same absorption maximum at 460 nm (Wellman & Jockusch, 2015). However, the band in the photodissociation spectrum due to loss of CO_2 was found to be narrower than the band for fluorescence emission. Power dependence measurements revealed that photodissociation required absorption of three photons while fluorescence was achieved with a single-photon excitation.

Action spectroscopy has been combined with Förster resonance energy transfer (FRET) in gas-phase ions tagged with fluorescent groups (Daly et al., 2014, 2018). This has been first applied to peptide polyalanine cations that were grafted at the N- and C-termini with QSY7 and carboxyrhodamine 575 (rh575) (Scheme 6) chromophores that showed different absorption maxima at 545 and 505 nm, respectively. Irradiation of the donor rh575 chromophore resulted in a dissociation of the receptor QSY7 chromophore providing evidence for electronic energy transfer. The FRET efficiency was shown to depend on the spacing between the donor and chromophore units that was varied by increasing the length of the peptide chain. An analogous FRET approach has also been used to study the conformations of gas-phase ions from amyloid peptides (Daly et al., 2015; Kulesza et al., 2016).

A different kind to energy transfer was investigated for peptides in which a cysteine residue was conjugated into a disulfide with 1-propanethiol (PT) or another cysteine-containing peptide (Hendricks et al., 2014). Peptides with aromatic residues (Trp, Tyr) showed photochemical cleavage of the S–S bond upon irradiation at wavelengths where Trp and Tyr strongly absorb, for example, at 290 and 266 nm, respectively. In contrast, peptides lacking these absorbers did not undergo photodissociation. Because disulfides do not strongly absorb light at these excitation wavelengths, the S–S bond photodissociation was attributed to a Dexter excitation energy transfer from the excited state of the aromatic chromophore to the disulfide.

9 | CIRCULAR DICHROIC ACTION SPECTRA

The structure information obtainable by UV-vis action spectroscopy has been further extended by measurements of circular dichroism of gas-phase DNA anions (Daly et al., 2020). Right-handed G-quadruplex ammonium complexes, D-$(dTGGGGT)_4(NH_4^+)_3$ (D-TG4T)) and their left-handed image L-$(dTGGGGT)_4(NH_4^+)_3$ (L-TG4T) were generated by electrospray as −5 ions in the gas phase and their action spectra were measured in the 230–295 nm

region by monitoring electron photodetachment (ePD). The irradiating laser beam was left or right circularly polarized, LCP or RCP, respectively. Circular dichroism was monitored as the wavelength-dependent relative difference in the photodetachment yields produced by the right-handed and left-handed laser beams, ($Yield^{LCP}$–$Yield^{RCP}$), that was expressed by factor g_{ePD} according to formula (1):

$$g_{ePD} = \frac{\Delta ePD}{ePD} = 2 \times \left(\frac{Yield_{ePD}^{LCP} - Yield_{ePD}^{RCP}}{Yield_{ePD}^{LCP} + Yield_{ePD}^{RCP}} \right). \quad (1)$$

The g_{ePD} plotted for the enantiomeric DNA ions showed opposite phases differing by 0.001%–0.002% that resembled similar phase differences in circular dichroism spectra in solution. The method was also applied to a mixture of other G-quadruplex penta-anions that were generated as complexes with potassium ions. Obviously, very careful measurements of ion photodetachment yields are critical in these experiments to distinguish the enantiomers.

10 | SUMMARY AND OUTLOOK

UV-vis action spectroscopy is applicable to a wide range of gas-phase polyatomic ions, providing information on their electronic structure. When applied to thermal ions, UV-vis is associated with band broadening because of unresolved vibrational states of polyatomic ions. This handicap can be removed or mitigated by cold-ion spectroscopy that can resolve vibrational states and provide vibrationally selected photodissociation to be further elaborated in depopulation (hole-burning) spectroscopy schemes such as in UV-IR. Despite being a low resolution method in the wavelength domain, UV-vis action spectroscopy enjoys some advantages against IR spectroscopy of gas-phase ions. First, the multichannel nature of UV-vis photodissociation allows one to monitor different fragment ion channels and thus obtain information on the excited electronic states accessed by photon absorption. The other favorable feature is that UV-vis excitation is mostly a single-photon process, which is advantageous for comparing experimental action spectra with calculated absorption spectra. Finally, structure features, such as strong hydrogen bonds, that result in large amplitude vibrations strongly affect band intensities in IR action spectra. Such effects are much less serious in UV-vis spectroscopy. This makes UV-vis action spectroscopy suitable for studying larger molecular systems, as documented for peptide and DNA cations and anions.

ACKNOWLEDGMENTS

The continuing support of author's research by the Chemistry Division of the National Science Foundation (Grant CHE-1951518) is gratefully appreciated. Thanks are due to my former and current group members Drs. Joseph A. Korn, Christopher J. Shaffer, Huong T. H. Nguyen, Emilie Viglino, Andy Dang, Yang Liu, Brandon Mozzone, Shu R. Huang, and Yue Liu for their invaluable contributions to UV-vis action spectroscopy. Graphics for Figure 3 was kindly provided by Professor Steen Brøndsted Nielsen and Dr. Jean Wyer of the University of Aarhus.

REFERENCES

Adamson BD, Coughlan NJA, Continetti RE, Bieske EJ. Changing the shape of molecular ions: photoisomerization action spectroscopy in the gas phase. *Phys. Chem. Chem. Phys.* 2013; *15*: 9540-9548.

Adamson BD, Coughlan NJA, Markworth PB, Continetti RE, Bieske EJ. An ion mobility mass spectrometer for investigating photoisomerization and photodissociation of molecular Ions. *Rev. Sci. Instrum.* 2014; *74*: 123109-1-123109-8.

Aguirre F, Husband J, Thompson CJ, Stringer KL, Metz RB. Electronic spectroscopy of intermediates involved in the conversion of methane to methanol by FeO^+. *J. Chem. Phys.* 2002; *116*: 4071-4078.

Alata I, Bert J, Broquier M, Dedonder C, Feraud G, Gregoire G, Soorkia S, Jouvet C. Electronic spectra of the protonated indole chromophore in the gas phase. *J. Phys. Chem. A* 2013; *117*: 4420–4427.

Allan M, Kloster-Jensen E, Maier JP. Emission spectra of the radical cations of diacetylene ($\sim A^2\Pi_u \rightarrow \sim X^2\Pi_g$), triacetylene ($\sim A^2\Pi_g \rightarrow \sim X^2\Pi_u$), and tetraacetylene ($\sim A^2\Pi_u \rightarrow \sim X^2\Pi_g$, 000), and the lifetimes of some vibronic levels of the ~A states. *Chem. Phys.* 1976; *17*: 11-18.

Allan M, Maier JP, Marthaler O, Kloster-Jensen E. Emission spectra of two $C_6H_6^+$ cations in the gas phase: competition of the radiative, ~A(π-1) → ~X(π-1), and fragmentation decay of the ~A(π-1) excited state of 2,4- and 1,3-hexadiyne radical cations. *Chem. Phys.* 1978; *29*: 331-337.

Andersen JU, Hvelplund P, Brøndsted Nielsen S, Tomita S, Wahlgreen H, Møller SP, Pedersen, UV, Forster JS, Jørgensen TJD. The combination of an electrospray ion source and an electrostatic storage ring for lifetime and spectroscopy experiments on biomolecules. *Rev. Sci. Instrum.* 2002,*73*, 1284-1287.

Antoine R, Dugourd P. UV-visible activation of biomolecular ions. (Laser photodissociation and spectroscopy of mass-separated biomolecular ions). *Lect. Notes Chem.* 2013; *83*: 93−116.

Ashfold MNR, King GA, Murdock D, Nix MGD, Oliver TAA, Sage AG. $\pi\sigma^*$ excited states in molecular photochemistry. *Phys. Chem. Chem. Phys.* 2010; *12*: 1218-1238.

Ashraf MA, Kozubal J, Metz RB. Bond dissociation energy and electronic spectroscopy of $Cr^+(NH_3)$ and its isotopomers. *J. Chem. Phys.* 2018; *149*: 174301/1-174301/6.

Baer T, Dunbar RC. Ion Spectroscopy: where did it come from; where is it now; and where is it going? *J. Am. Soc. Mass Spectrom.* 2010; *21*: 681-693.

Bakels S, Meijer EM, Greuell M, Porskamp SBA, Rouwhorst G, Mahe J, Gaigeot MP, Rijs AM. Interactions of aggregating peptides probed by IR-UV action spectroscopy. *Faraday Discuss*. 2019; *217*: 322-341.

Barbatti M, Ruckenbauer M, Plasser F, Pittner J, Granucci G, Persico M, Lischka H. Newton-X: a surface-hopping program for nonadiabatic molecular dynamics. *Wiley Interdiscip. Rev. Comput. Mol. Sci.* 2014; *4*: 26−33.

Batalov A, Fulara J, Shnitko I, Maier JP. Electronic absorption spectra of the protonated polyacetylenes $H_2C_nH^+$ (n = 4, 6, 8) in neon matrixes. *J. Phys. Chem. A.* 2006; *110*: 10404-10408.

Berdakin M, Féraud G, Dedonder-Lardeux C, Jouvet C, Pino GA. Excited states of protonated DNA/RNA bases. *Phys. Chem. Chem. Phys.* 2014; *16*: 10643-10650.

Bieske EJ, Dopfer O. High-resolution spectroscopy of cluster ions. *Chem. Rev.* 2000; *100*: 3963-3998.

Bochenkova AV, Mooney CRS, Parkes MA, Woodhouse JL, Zhang L, Lewin R, Ward JM, Hailes HC, Andersen LH, Fielding HH. Mechanism of resonant electron emission from the deprotonated GFP chromophore and its biomimetics. *Chem. Sci.* 2017; *8*: 3154-3163.

Bondybey VE, Miller TA, English JH. Electronic absorption spectra of molecular cations. *J. Chem. Phys.* 1980; *72*: 2193-2194.

Booth RS, Annesley CJ, Young JW, Vogelhuber KM, Boatz JA, Stearns, JA. Identification of multiple conformers of the ionic liquid [emim][tf2n] in the gas phase using IR/UV action spectroscopy. *Phys. Chem. Chem. Phys.* 2016; *18*: 17037-17043.

Brodbelt JS, Morrison LJ, Santos I. Ultraviolet photodisociation mass spectrometry for analysis of biological molecules. *Chem Rev*. 2020; *120*: 3328-3380.

Bull JN, Carrascosa E, Giacomozzi L, Bieske EJ, Stockett MH. Ion mobility action spectroscopy of flavin dianions reveals deprotomer-dependent photochemistry. *Phys. Chem. Chem. Phys.* 2018; *20*: 19672-19681.

Bull JN, Scholz MS, Coughlan NJA, Bieske EJ. Isomerisation of an intramolecular hydrogen-bonded photoswitch: protonated azobis (2-imidazole). *Phys. Chem. Chem. Phys.* 2017; *19*: 12776-12783.

Bull JN, da Silva G, Scholz MS, Carrascosa E, Bieske EJ. Photo-initiated intramolecular proton transfer in deprotonated para-coumaric acid. *J. Phys. Chem. A.* 2019; *123*: 4419-4430.

Burke NL, Redwine JG, Dean JC, McLuckey SA, Zwier TS. UV and IR spectroscopy of cold protonated leucine encephalin. *Int. J. Mass Spectrom.* 2015; *378*: 196-205.

Caricato M, Trucks GW, Frisch MJ, Wiberg KB. Electronic transition energies: a study of the performance of a large range of single reference density functional and wave function methods on valence and Rydberg states compared to experiment. *J. Chem. Theory Comput.* 2010; *6*: 370−383.

Catani KJ, Muller G, Jusko P, Theule P, Bieske EJ, Jouvet C. Electronic spectrum of the protonated diacetylene cation ($H_2C_4H^+$). *J. Chem. Phys.* 2017; *147*: 084302/1-084302/5.

Cheong NR, Nam SH, Park HS, Ryu S, Song JK, Park SM, Pérot M, Lucas B, Barat M, Fayeton JA, Jouvet C. Photofragmentation in selected tautomers of protonated adenine. *Phys. Chem. Chem. Phys.* 2011; *13*: 291–295.

Choi CM, Kim HJ, Lee JH, Shin WJ, Yoon TO, Kim NJ, Heo J. Ultraviolet photodepletion spectroscopy of dibenzo-18-crown-6-ether complexes with alkali metal cations. *J. Phys. Chem. A*. 2009; *113*: 8343–8350.

Citir M, Altinay G, Metz RB. Electronic and vibrational spectroscopy and vibrationally mediated photodissociation of $V^+(OCO)$. *J. Phys. Chem. A.* 2006; *110*: 5051-5057.

Cornett DS, Peschke M, LaiHing K, Cheng PY,Willey KF, Duncan MA. Reflectron time-of-flight mass spectrometer for laser photodissociation. *Rev. Sci. Instrum.* 1992; *63*: 2177–2186.

Coughlan NJA, Catani KJ, Adamson BD, Wille U, Bieske EJ. Photoisomerization action spectrum of retinal protonated Schiff base in the gas phase. *J. Chem. Phys.* 2014; *140*: 164307/1-164307/10.

Coughlan NJA, Scholz MS, Hansen CS, Trevitt AJ, Adamson BD, Bieske EJ. Photo and collision induced isomerization of a cyclic retinal derivative: an ion mobility study. *J. Am. Soc. Mass Spectrom.* 2016; *27*: 1483-1490.

Crabtree RH. Aspects of methane chemistry. *Chem. Rev.* 1995; *95*: 987-1007.

Daluz JS, Kocak A, Metz RB. Photodissociation Studies of the Electronic and Vibrational Spectroscopy of $Ni^+(H_2O)$. *J. Phys. Chem. A*. 2012; *116*: 1344-1352.

Daly S, Kulesza A, Knight G, MacAleese L, Antoine R, Dugourd P. Visible and ultraviolet spectroscopy of gas phase rhodamine 575 cations. *J. Phys. Chem. A.* 2015; *119*: 5634-5641.

Daly S, Kulesza A, Poussigue F, Simon AL, Choi CM, Knight G, Chirot F, MacAleese L, Antoine R, Dugourd P. Conformational changes in amyloid-beta (12-28) alloforms studied using action-FRET, IMS and molecular dynamics simulations. *Chem. Sci.* 2015; *6*: 5040-5047.

Daly S, MacAleese L, Dugourd P, Chirot F. Combining structural probes in the gas phase-ion mobility-resolved action-FRET. *J. Am. Soc. Mass Spectrom.* 2018; *29*: 133-139.

Daly S, Porrini M, Rosu F, Gabelica V. Electronic spectroscopy of isolated DNA polyanions. *Faraday Discuss*. 2019; *217*: 361-382.

Daly S, Poussigue F, Simon AL, MacAleese L, Bertorelle F, Chirot F, Antoine R, Dugourd P. Action-FRET: probing the molecular conformation of mass-selected gas-phase peptides with Forster resonance energy transfer detected by acceptor-specific fragmentation. *Anal. Chem.* 2014; *86*: 8798-8804.

Daly S, Rosu F, Gabelica V. Mass-resolved electronic circular dichroism ion spectroscopy. *Science.* 2020; *368*(6498): 1465-1468.

Dang A, Korn JA, Gladden J, Mozzone B, Tureček F. UV-Vis photodissociation action spectroscopy on Thermo LTQ-XL ETD and Bruker amaZon ion trap mass spectrometers: a practical guide. *J. Am. Soc. Mass Spectrom.* 2019; *30*: 1558-1564.

Dang A, Liu Y, Tureček F. UV-Vis action spectroscopy of guanine, 9-methylguanine and 2′-deoxyguanosine cation radicals in the gas phase. *J. Phys. Chem. A* 2019; *123*: 3272-3284.

Dang A, Nguyen HTH, Ruiz H, Piacentino E, Ryzhov V, Tureček F. Experimental evidence for non-canonical thymine cation radicals in the gas phase. *J. Phys. Chem. B.* 2018; *122*: 86-97.

Dang A, Shaffer CJ, Bím D, Lawler J, Lesslie M, Ryzhov V. Tureček, F.: Near-UV water splitting by Cu, Ni, and Co complexes in the gas phase. *J. Phys. Chem. A.* 2018; *122*: 2069-2078.

Ding H, Pino T, Guethe F, Maier JP. Isomeric structures and visible electronic spectrum of the C_7H_3 radicals. *J. Am. Chem. Soc.* 2003; *125*: 14626-14630.

Dodson LG, Zagorec-Marks W, Xu S, Smith JET, Weber JM. Intrinsic photophysics of nitrophenolate ions studied by

cryogenic ion spectroscopy. *Phys. Chem. Chem. Phys.* 2018; *20*: 28535-28543.

Douix S, Dossmann H, Nicol E, Duflot D, Giuliani A. Spectroscopy and photodissociation of perfluorooctanoate anion. *Chem. Eur. J.* 2018; *24*: 15572-15576.

Drink E, Dugourd P, Dumont E, Aronssohn N, Antoine R, Loison C. Optical properties of prodigiosin and obatoclax: action spectroscopy and theoretical calculations. *Phys. Chem. Chem. Phys.* 2015; *17*: 25946-25955.

Dunbar RC. Photodissociation of the methyl chloride (CH_3Cl^+) and nitrous oxide (N_2O^+) cations. *J. Am. Chem. Soc.* 1971; *93*: 4354–4358.

Duncan MA. Spectroscopy of metal ion complexes: gas-phase models for solvation. *Ann. Rev. Phys. Chem.* 1997; *48*: 69-93.

Dzvonik M, Yang S, Bersohn R. Photodissociation of molecular beams of aryl halides. *J. Chem. Phys.* 1974; *61*: 4408-4421.

Egashira K, Terasaki A. Optical absorption spectrum of the chromium dimer cation: measurements by photon-trap and photodissociation spectroscopy. *Chem. Phys. Lett.* 2015; *635*: 13-15.

Elm J, Stockett M, Houmoeller J, Aaxman PM, Mikkelsen K, Nielsen MB, Nielsen SB. Gas-phase spectroscopy of a vinylheptafulvene chromophore. *Eur. J. Mass Spectrom.* 2015; *21*: 569-577.

Enjalbert Q, Brunet C, Vernier A, Allouche AR, Antoine R, Dugourd P, Lemoine J, Giuliani A, Nahon L. Vacuum ultraviolet action spectroscopy of polysaccharides. *J. Am. Soc. Mass Spectrom.* 2013; *24*: 1271-1279.

Eyler JR Infrared multiple photo dissociation spectroscopy of ions in Penning traps. *Mass Spectrom. Rev.* 2009; *28*: 448–467.

Faherty KP, Thompson CJ, Aguirre F, Michne J, Metz RB. Electronic Spectroscopy and Photodissociation Dynamics of Hydrated Co^{2+} Clusters: $Co^{2+}(H_2O)_n$ (n = 4-7). *J. Phys. Chem. A.* 2001; *105*: 10054-10059.

Feraud G, Berdakin M, Dedonder C, Jouvet C, Pino GA. Excited states of proton-bound DNA/RNA base homodimers: pyrimidines. *J. Phys. Chem. B.* 2015; *119*: 2219-2228.

Feraud G, Dedonder C, Jouvet C, Inokuchi Y, Haino T, Sekiya R, Ebata T. Development of ultraviolet hole-burning spectroscopy for cold gas-phase ions. *J. Phys. Chem. Lett.* 2014; *5*: 1236−1240.

Feraud G, Dedonder-Lardeux C, Jouvet C, Marceca E. Photodissociation UV-Vis spectra of cold protonated azobenzene and 4-(dimethylamino)azobenzene and their benzenediazonium cation fragment. *J. Phys. Chem. A*. 2016; *120*: 3897-3905.

Feraud G, Esteves-Lopez N, Dedonder-Lardeux C, Jouvet C. UV spectroscopy of cold ions as a probe of the protonation site. *Phys. Chem. Chem. Phys.* 2015; *17*: 25755-25760.

Foerstel M, Pollow KM, Saroukh K, Najib EA, Mitric R, Dopfer O. The optical spectrum of Au_2^+ *Angew. Chem. Int. Ed.* 2020; *59*: 21403-21408.

Forbes MW, Jockusch RA. Deactivation pathways of an isolated green fluorescent protein model chromophore studied by electronic action spectroscopy. *J. Am. Chem. Soc.* 2009; *131*: 17038-17039.

Forbes MW, Jockusch RA. Gas-phase fluorescence excitation and emission spectroscopy of three xanthene dyes (rhodamine 575, rhodamine 590 and rhodamine 6G) in a quadrupole ion trap mass spectrometer. *J. Am. Soc. Mass Spectrom.* 2011; *22*: 93-109.

Forbes MW, Nagy AM, Jockusch RA. Photofragmentation of and electron photodetachment from a GFP model chromophore in a quadrupole ion trap. *Int. J. Mass Spectrom.* 2011; *308*: 155-166.

Forbes MW, Talbot FO, Jockusch RA. 2009. The spectroscopy of ions stored in trapping mass spectrometers. In: March RE, Todd JFJ., Editors. *Practical Aspects of Trapped Ion Mass Spectrometry*, 5, Chapter 9, Boca Raton, FL: CRC Press. pp. 239-290.

Forney D, Jakobi M, Maier JP. Absorption spectroscopy of mass-selected ions in neon matrixes. *J. Chem. Phys.* 1989; *90*: 600-601.

Fujihara A, Matsumoto H, Shibata Y, Ishikawa H, Fuke K. Photodissociation and spectroscopic study of cold protonated dipeptides. *J. Phys. Chem. A.* 2008; *112*: 1457–1463.

Fulara J, Chakraborty A, Maier JP. Electronic characterization of reaction intermediates: the fluorenylium, phenalenylium, and benz[f]indenylium cations and their radicals. *Angew. Chem. Int. Ed.* 2016; *55*: 3424-3427.

Fulara J, Erattupuzha S, Garkusha I, Maier JP. Structure and electronic transitions of $C_7H_4O_2^+$ and $C_7H_5O_2^+$ ions: neon matrix and theoretical studies. *J. Phys. Chem. A.* 2016; *120*: 10134-10140.

Furche F, Ahlrichs R. Adiabatic time-dependent density functional methods for excited state properties. *J. Chem. Phys.* 2002; *117*: 7433−7447.

Gatchell M, Martini P, Laimer F, Goulart M, Calvo F, Scheier P. Spectroscopy of corannulene cations in helium nanodroplets. *Faraday Discuss.* 2019; *217*: 276-289.

Gonzalez L, Escudero D, Serrano-Andres L. Progress and challenges in the calculation of electronic excited states. *ChemPhysChem.* 2012; *13*: 28−51.

Gunzer F, Kruger S, Grotemeyer J. Photoionization and photofragmentation in mass spectrometry with visible and UV lasers. *Mass Spectrom Rev*. 2019; *38*: 202–217.

Hait D, Head-Gordon M. Orbital optimized density functional theory for electronic excited states. *J Phys Chem Lett*. 2021; *12*: 4517–4529.

Hansen CS, Blanskby SJ, Trevitt AJ. Ultraviolet action spectroscopy of gas-phase protonated quinoline and isoquinoline cations. *Phys. Chem. Chem. Phys.* 2015; *17*: 25882-25890.

Hansen CS, Kirk B, Blanksby SJ, O'Hair RAJ, Trevitt AJ. UV photodissociation action spectroscopy of haloanilinium ions in a linear quadrupole ion trap mass spectrometer. *J. Am. Soc. Mass Spectrom.* 2013; *24*: 932-940.

Hansen CS, Kirk BB, Blanksby SJ, Trevitt AJ. Ultraviolet photodissociation of the N-methylpyridinium ion: action spectroscopy and product characterization. *J. Phys. Chem. A.* 2013; *117*: 10839-10846.

Hansen K. Action spectroscopy of highly excited molecular ions in molecular beams. *Int. J. Mass Spectrom.* 2018; *430*: 14-21.

Hendricks, NG, Lareau NM, Stow SM, McLean JA, Julian RR. Bond-specific dissociation following excitation energy transfer for distance constraint determination in the gas phase. *J. Am. Chem. Soc.* 2014; *136*: 13363-13370.

Herve M, Bredy R, Karras G, Concina B, Brown J, Allouche AR, Lepine F, Compagnon I. On-the-fly femtosecond action spectroscopy of charged cyanine dyes: electronic structure versus geometry. *J. Phys. Chem. Lett.* 2019; *10*: 2300-2305.

Hettich RL, Freiser BS. Gas-Phase Photodissociation of $FeCH_2^+$ and $CoCH_2^+$: Determination of the Carbide, Carbyne, and Carbene Bond Energies. *J. Am. Chem. Soc.* 1986; *108*: 2537-2540.

Hoffmann B, Esser TK, Abel B, Asmis KR. Electronic action spectroscopy on single nanoparticles in the gas phase. *J. Phys. Chem. Lett.* 2020; *11*: 6051-6056.

Hoshika S, Leal NA, Kim MJ, Kim MS, Karalkar NB, Kim HJ, Bates AM, Watkins NE, Jr. SantaLucia HA, Meyer AJ, DasGupta S, Piccirilli JA, Ellingotn AD, SantaLucia J, Jr., Georgiadis MM, Benner SA. Hachimoji DNA and RNA: A genetic system with eight building blocks. *Science.* 2019; *363*: 884−887.

Huang SR, Dang A, Tureček F. Ground and excited states of gas-phase DNA nucleobase cation-radicals. A UV-vis photodisociation action spectroscopy and computational study of adenine and 9-methyladenine. *J. Am. Soc. Mass Spectrom.* 2020; *31*: 1271-1281.

Huang SR, Kiu Y, Turecek F. UV-vis photodissociation action spectroscopy reveals cytosine-guanine hydrogen transfer in DNA tetranucleotide catio radiclas upon one-electron reduction. *J. Phys. Chem. B.* 2020; *124*: 3505-3517.

Huang SR, Nováková G, Marek A, Tureček F. The elusive non-canonical isomers of ionized 9-methyladenine and 2′-deoxyadenosine. *J. Phys. Chem. A*. 2021; *125*: 338-348.

Huang SR, Tureček F. Cation radicals of hachimoji nucleobases. Canonical purine and non-canonical pyrimidine forms generated in the gas phase and characterized by UV-vis photodissociation action spectroscopy. *J. Phys. Chem. A.* 2020; *124*: 7101-7112.

Huang SR, Tureček F. Cation radicals of hachimoji nucleobases P and Z. Generation in the gas phase and characterization by UV-vis photodissociation action spectroscopy and theory. *J. Am. Soc. Mass Spectrom.* 2021; *32*: 373-386.

Husband J, Aguirre F, Ferguson P, Metz RB. Vibrationally resolved photfragment spwectroscopy of FeO^+. *J. Chem. Phys.* 1999; *111*: 1433-1436.

Hutter D, Benner SA. Expanding the genetic alphabet: non-epimerizing nucleoside with the pyDDA hydrogen-bonding pattern. *J. Org. Chem.* 2003; *68*: 9839−9842.

Imaoka N, Houferak C, Murphy MP, Nguyen HTH, Dang A, Tureček F. Spontaneous isomerization of peptide cation radicals following electron transfer dissociation revealed by UV-vis photodissociation action spectroscopy. *J. Am. Soc. Mass Spectrom.* 2018; *29*: 1768-1780.

Inokuchi Y, Haino T, Sekiya R, Morishima F, Dedonder C, Feraud G, Jouvet C, Ebata T. UV photodissociation spectroscopy of cryogenically cooled gas phase host-guest complex ions of crown ethers. *Phys. Chem. Chem. Phys.* 2015; *17*: 25925-25934.

Jasik J, Navratil R, Nemec I, Roithova J. Infrared and visible photodissociation spectra of rhodamine ions at 3 K in the gas phase. *J. Phys. Chem. A.* 2015; *119*: 12648-12655.

Johnston MD, Gentry MR, Metz RB. Photofragment imaging, spectroscopy, and theory of MnO^+. *J. Phys. Chem. A.* 2018; *122*: 8047-8053.

Johnston MD, Pearson WL, III, Wang G, Metz RB. A velocity map imaging mass spectrometer for photofragment of fast ion beams. *Rev. Sci. Instrum.* 2018; *89*: 014102.

Kirk BB, Trevitt AJ, Blanksby SJ, Tao Y, Moore BN, Julian RR. Ultraviolet action spectroscopy of iodine labeled peptides and proteins in the gas phase. *J. Phys. Chem. A.* 2013; *117*: 1228-1232.

Kirketerp MBS, Nielsen SB. Absorption spectrum of isolated tris (2,2′-bipyridine)ruthenium(II) dications in vacuo. *Int. J. Mass Spectrom.* 2010; *297*: 63–66.

Klaerke B., Holm AIS, Andersen LH. UV action spectroscopy of protonated PAH derivatives: methyl substituted quinolones. *Astronomy Astrophys.* 2011; *532*: A132/1-A132/5.

Kocak A, Austein-Miller G, Pearson WL, Altinay G, Metz RB. Dissociation energy and electronic and vibrational spectroscopy of $Co^+(H_2O)$ and its isotopomers. *J. Phys. Chem. A.* 2013; *117*: 1254-1264.

Korn JA, Urban J, Dang A, Nguyen HTH, Turecek F. UV-vis action spectroscopy reveals a conformational collapse in hydrogen-rich dinucleotide cation radicals. *J. Phys. Chem. Lett.* 2017; *8*: 4100-4107.

Kulesza A, Daly S, Choi CM, Simon AL, Chirot F, MacAleese L, Antoine R, Dugourd P. The structure of chromophore-grafted amyloid-β12-28 dimers in the gas-phase: FRET-experiment guided modelling. *Phys. Chem. Chem. Phys.* 2016; *18*: 9061-9069.

Laurent AD, Jacquemin D. TD-DFT Benchmarks: A review. *Int. J. Quantum Chem*. 2013, *113*, 2019−2039.

Leang SS, Zahariev F, Gordon MS. Benchmarking the performance of time-dependent density functional methods. *J. Chem. Phys.* 2012; *136*: 104101/1−10410112.

Lemmens AK, Rap DB, Thunnissen JMM, Willemsen B, Rijs AM, Polycyclic aromatic hydrocarbon formation chemistry in a plasma jet revealed by IR-UV action spectroscopy. *Nature Commun*. 2020; *11*: 269.

Lessen D, Brucat PJ. Resonant photodissociation of $CoAr^+$ and $CoKr^+$: Analysis of vibrational structure. *J. Chem. Phys.* 1989; *90*: 6296-6305.

Lessen D, Brucat PJ. Characterization of transition metal-rare-gas cations:VAr^+ and VKr^+. *J. Chem. Phys.* 1989; *91*: 4522-4530.

Lesslie M, Lawler JT, Dang A, Korn JA, Bím D, Steinmetz V, Maitre P, Tureček F, Ryzhov V. Cytosine radical cation: a gas-phase study combining IRMPD spectroscopy, UV-PD spectroscopy, ion-molecule reactions, and theoretical calculations. *ChemPhysChem.* 2017; *18*: 1293-1301.

Leutwyler S, Maier JP, Spittel U. The electronic absorption spectrum of the diiododiacetylene cation ($I\text{-}C{\equiv}C\text{-}C{\equiv}C\text{-}I^+$) in a neon matrix. *Chem. Phys. Lett.* 1983; *96*: 645-648.

Lincke K, Langeland J, Madsen AO, Kiefer HV, Skov L, Gruber E, Mikkelsen KV, Andersen LH, Nielsen MB. Elucidation of the intrinsic optical properties of hydrogen-bonded and protonated flavin chromophores by photodissociation action spectroscopy. *Phys. Chem. Chem. Phys.* 2018; *20*: 28678-28684.

Liu Y, Dang A, Urban J, Tureček F. Charge-tagged DNA radicals in the gas phase characterized by UV-vis photodissociation action spectroscopy. *Angew. Chem. Int. Ed. Engl.* 2020; *59*: 7772-7777.

Liu Y, Huang SR, Tureček F. Guanine-adenine interactions in DNA tetranucleotide cation radicals revealed by UV/vis photodissociation action spectroscopy and theory. *Phys. Chem. Chem. Phys.* 2020; *22*: 16831-16842.

Liu Y, Korn JA, Dang A, Turecek F. Hydrogen-rich cation radicals of DNA dinucleotides. Generation and structure elucidation

by UV-vis action spectroscopy. *J. Phys Chem. B.* 2018; *122*: 9665-9680.

Liu Y, Korn JA, Turecek F. UV-vis action spectroscopy and structures of hydrogen-rich 2′-deoxycytidine dinucleotide cation radicals. A difficult case. *Int. J. Mass Spectrom.* 2019; *443*: 22-31.

Liu Y, Ma C, Leonen CJA, Chatterjee C, Nováková G, Marek A, Tureček F. Tackling a curious case. Generation of charge-tagged guanosine radicals by electron transfer in the gas phase and their characterization by UV-vis photodissociation action spectroscopy and theory. *J. Am. Soc. Mass Spectrom.* 2021; *32*: 772-785.

Liu Y, Ma C, Nováková G, Marek A, Tureček F. Charge-tagged nucleosides in the gas phase: UV-vis action spectroscopy and structures of cytidine cations, dications and cation radicals. *J. Phys. Chem. A* 2021; *125*, 6096-6108. https://doi.org/10.1021/acs.jpca.1c03477

Maier JP. Open-shell organic cations: spectroscopic studies by means of their radiative decay in the gas phase. *Acc. Chem. Res.* 1982; *15*: 18-23.

Maier JP. Spectroscopic structure of open-shell polyatomic cations. *Chem. Soc. Rev.* 1988, *17*, 45-67.

Maier JP. Approaches to spectroscopic characterization of cations *Int. J. Mass Spectrom. Ion Processes.* 1991; *104*: 1-22.

Maier JP, Thommen F. Fluorescence quantum yields and lifetimes of fluorobenzene cations in selected levels of their B~ and C~ states determined by photoelectron-photon coincidence spectroscopy. *Chem. Phys.* 1981; *57*: 319-332.

Marian C, Nolting D, Weinkauf R. The electronic spectrum of protonated adenine: theory and experiment. *Phys. Chem. Chem. Phys.* 2005; *7*: 3306−3316.

Markworth PB, Adamson BD, Coughlan NJA, Goerigk L, Bieske EJ. Photoisomerization action spectroscopy: flicking the protonated merocyanine-spiropyran switch in the gas phase. *Phys. Chem. Chem. Phys.* 2015; *17*: 25676-25688.

Marlton SJP, McKinnon BI, Ucur B, Bezzina JP, Blanksby SJ, Trevitt AJ. Discrimination between protonation isomers of quinazoline by ion mobility and UV-photodissociation action spectroscopy. *J. Phys. Chem. Lett.* 2020; *11*: 4226-4231.

Marlton SJP, McKinnon BI, Ucur B, Maccarone AT, Donald WA, Blanksby SJ, Trevitt AJ. Electronic spectroscopy of isolated DNA polyanions. *Faraday Discuss*. 2019; *217*: 453-475.

Matthews E, Dessent CEH. Locating the proton in nicotinamide protomers via low-resolution UV action spectroscopy of electrosprayed solutions. *J. Phys. Chem. A* 2016; *120*: 9209–9216.

McLafferty FW, Turecek F. 1993. *Interpretation of Mass Spectra*, 4th Edition, Mill Valley, CA: University Science Books.

McLaughlin C, Assmann M, Parkes MA, Woodhouse JL, Lewin R, Hailes HC, Worth GA, Fielding HH. Ortho and para chromophores of green fluorescent protein: controlling electron emission and internal conversion. *Chem. Sci.* 2017; *8*: 1621-1630.

Metz RB. Photofragment spectroscopy of covalently bound transition metal complexes: a window into C-H and C-C bond activation by transition metal ions. *Int. Rev. Phys. Chem.* 2004; *23*: 79-108.

Metz RB. Optical spectroscopy and photodissociation dynamics of multiply charged ions. *Int. J. Mass Spectrom.* 2004; *235*: 131-143.

Metz RB, Altinay G, Kostko O, Ahmed M. Probing reactivity of gold atoms with acetylene and ethylene with VUV photoionization mass Spectrometry and ab initio studies. *J. Phys. Chem. A*. 2019; *123*: 2194-2202.

Milosavljevic AR, Nicolas C, Gil JF, Canon F, Réfrégiers M, Nahon L, Giuliani A. VUV synchrotron radiation: a new activation technique for tandem mass spectrometry. *J. Synchrotron Radiat.* 2012; *19*: 174-178.

Milosavljevic AR, Nicolas C, Lemaire J, Dehon C, Thissen R, Bizau JM, Réfrégiers M, Nahon L, Giuliani A. Photoionization of a protein isolated in vacuo. *Phys. Chem. Chem. Phys.* 2011; *13*: 15432-15436.

Mooney CRS, Sanz ME, McKay AR, Fitzmaurice RJ, Aliev AE, Caddick S, Fielding HH. Photodetachment spectra of deprotonated fluorescent protein chromophore anions. *J. Phys. Chem. A.* 2012; *116*: 7943-7949.

Mueller D, Dopfer O. Vibronic optical spectroscopy of cryogenic flavin ions: the O2+ and N1 tautomers of protonated lumiflavin. *Phys. Chem. Chem. Phys.* 2020; *22*: 18328-18339.

Musbat L, Assis S, Dilger JM, El-Baba TJ, Fuller DR, Knudsen JL, Kiefer HV, Hirshfeld A, Friedman N, Andersen LH, Sheves M, Clemmer DE, Toker Y. Action and ion mobility spectroscopy of a shortened retinal derivative. *J. Am. Soc. Mass Spectrom.* 2018; *29*: 2152-2159.

Navratil R, Jasik J, Roithova J. Visible photodissociation spectra of gaseous rhodamine ions: Effects of temperature and tagging. *J. Mol. Spectrosc.* 2017; *332*: 52-58.

Nguyen HTH, Andrikopoulos PC, Bím D, Rulíšek L, Dang A, Tureček F. Radical reactions affecting polar groups in threonine peptide ions. *J. Phys. Chem. B.* 2017; *121*: 6557-6569.

Nguyen, HTH, Shaffer CJ, Pepin R, Tureček F. UV action spectroscopy of gas-phase peptide radicals. *J. Phys. Chem. Lett.* 2015; *6*: 4722-4727.

Noble JA, Broquier M, Gregoire G, Soorkia S, Pino G, Marceca E, Dedonder-Lardeux C, Jouvet C. Tautomerism and electronic spectroscopy of protonated 1- and 2-aminonaphthalene. *Phys. Chem. Chem. Phys.* 2018; *20*: 6134-6145.

Nolting D, Marian CM, Weinkauf R. Protonation effect on the electronic spectrum of tryptophan in the gas phase. *Phys. Chem. Chem. Phys.* 2004; *6*: 2633-2640.

Nolting D, Schultz T, Hertel IV, Weinkauf R. Excited state dynamics and fragmentation channels of the protonated dipeptide H2N-Leu-Trp-COOH. *Phys. Chem. Chem. Phys.* 2006; *8*: 5247-5254.

Nolting D, Weinkauf R, Hertel IV, Schultz T. Excited-State Relaxation of Protonated Adenine. *ChemPhysChem.* 2007; *8*: 751−755.

Peach MJG, Benfield P, Helgaker T, Tozer DJ. Excitation energies in density functional theory: an evaluation and a diagnostic test. *J. Chem. Phys.* 2008; *128*: 044118/1−044118/8.

Pearson WL, Copeland C, Kocak A, Sallese Z, Metz RB. Near ultraviolet photodissociation spectroscopy of $Mn^+(H_2O)$ and $Mn^+(D_2O)$. *J. Chem. Phys.* 2014; *141*: 204305/1-204305/9.

Pedersen BM, Nielsen SB. Gas-phase ion spectroscopy of flexible and nonflexible nitrophenolates: effect of locking the two phenyl units in 4′-nitro-[1,1′-biphenyl]-4-olate by a bridging atom. *J. Self-Assembly Mol. Electron.* 2018; *6*: 1-12.

Pedersen SØ, Byskov CS; Turecek F, Nielsen SB. Structures of protonated thymine and uracil and their monohydrated gas-

phase ions from ultraviolet action spectroscopy and theory. *J. Phys. Chem. A*. 2014; *118*: 4256-4265.

Pedersen SØ, Støchkel K, Byskov CS, Baggesen LM, Brøndsted Nielsen S. Gas-phase spectroscopy of protonated adenine, adenosine 5′-monophosphate and monohydrated Ions. *Phys. Chem. Chem. Phys.* 2013; *15*: 19748−19752.

Pepin R, Layton ED, Liu Y, Afonso C, Tureček F. Where does the electron go? Stable and metastable peptide cation radicals formed by electron transfer. *J. Am. Soc. Mass Spectrom.* 2017; *28*: 164-181.

Perera KM, Metz RB. Photodissociation spectroscopy and dissociation dynamics of $TiO^+(CO_2)$ *J. Phys. Chem. A*. 2009; *113*: 6253-6259.

Perera M, Ganssle P, Metz RB. Microsolvation of Co2+ and Ni2+ by acetonitrile and water: photodissociation dynamics of $M^{2+}(CH_3CN)_n(H_2O)_m$. *Phys. Chem. Chem. Phys.* 2011; *13*: 18347-18354.

Polfer NC. Infrared multiple photon dissociation spectroscopy of trapped ions. *Chem. Soc. Rev.* 2011; *40*: 2211−2221.

Polfer NC, Dugourd P, Eds. *Laser Photodissociation and Spectroscopy of Mass Separated Biomolecular Ions; Lecture Notes in Chemistry*; Springer: Cham, 2013; 83, pp 13−20.

Rankovic ML, Canon F, Nahon L, Giuliani A, Milosavljevic AR. VUV action spectroscopy of protonated leucine-enkephalin peptide in the 6-14 eV range. *J. Chem. Phys.* 2015; *143*: 244311/1-244311/8.

Rankovic ML, Giuliani A, Milosavljevic AR. Design and performance of an instrument for electron impact tandem mass spectrometry and action spectroscopy of mass/charge selected macromolecular ions stored in RF ion trap. *Eur. Phys. J. D: Atomic Mol. Optical Plasma Phys.* 2016; *70*: 1-11.

Riffet V, Jacquemin D, Cauet E, Frison G. Benchmarking DFT and TD-DFT functionals for the ground and excited states of hydrogen-rich peptide radicals. *J. Chem. Theory Comput.* 2014; *10*: 3308−3318.

Rizzo TR, Stearns JA, Boyarkin OV. Spectroscopic studies of cold, gas-phase biomolecular ions. *Int. Rev. Phys. Chem.* 2009; *28*: 481-515.

Shaffer CJ, Pepin R, Tureček F. Combining UV photodissociation action spectroscopy with electron transfer dissociation for structure analysis of gas-phase peptide cation-radicals. *J. Mass Spectrom.* 2015; *50*: 1438-1442.

Sheldrick A, Mueller D, Guenther A, Nieto P, Dopfer O. Optical spectroscopy of isolated flavins: photodissociation of protonated lumichrome. *Phys. Chem. Chem. Phys.* 2018; *20*: 7407-7414.

Silva-Junior MR, Schreiber M, Sauer SPA, Thiel W. Benchmarks for electronically excited states: time-dependent density functional theory and density functional theory based multireference configuration interaction. *J. Chem. Phys.* 2008; *129*: 104103/1−104103/14.

Singh PC, Patwari GN. IR-UV double resonance spectroscopic investigation of phenylacetylene-alcohol complexes. Alkyl group induced hydrogen bond switching. *J. Phys. Chem. A*. 2008; *112*: 5121-5125.

Sonk KA, Schlegel HB. RD-CI Simulation of the electronic optical response of molecules in intense fields II: comparison of DFT functionals and EOM-CCSD. *J. Phys. Chem. A*. 2011; *115*: 11832−11840.

Soorkia S, Jouvet C, Gregoire G. UV photoinduced dynamics of conformer-resolved aromatic peptides. *Chem. Rev.* 2020; *120*: 3296-3327.

Srnec M, Navratil R, Andris E, Jasik J, Roithova J. Experimentally calibrated analysis of the electronic structure of CuO+: implications for reactivity. *Angew. Chem. Int. Ed.* 2018; *57*: 17053-17057.

Stockett MH, Broendsted Nielsen S. Does a single CH3CN molecule attached to Ru(bipy)32+ affect its absorption spectrum? *J. Chem. Phys.* 2015; *142*: 171102/1-171102/4.

Stockett MH, Houmoeller J, Stoechkel K, Svendsen A, Broendsted Nielsen S. A cylindrical quadrupole ion trap in combination with an electrospray ion source for gas-phase luminescence and absorption spectroscopy. *Rev Sci Instrum*. 2016; *87*: 053103/1-053103/9.

Stringer KL, Citir M, Metz RB. Photofragment Spectroscopy of π Complexes: $Au^+(C_2H_4)$ and $Pt^+(C_2H_4)$. *J. Phys. Chem. A*. 2004; *108*: 6996-7002.

Støchkel K, Milne BF, Brøndsted Nielsen S. Absorption spectrum of the firefly luciferin anion isolated in vacuo. *J. Phys. Chem. A*. 2011; *115*: 2155−2159.

Svendsen A, Lorenz UJ, Boyarkin OV, Rizzo TR. A new tandem mass spectrometer for photofragment spectroscopy of cold, gas-phase molecular ions. *Rev. Sci. Instrum.* 2010; *81*: 073107/1-073107/7.

Syka JEP, Coon JJ, Schroeder MJ, Shabanowitz J, Hunt DF. Peptide and protein sequence analysis by electron transfer dissociation mass spectrometry. *Proc. Natl. Acad. Sci. USA*. 2004; *101*: 9528–9533.

Tesler LF, Cismesia AP, Bell MR, Bailey LS, Polfer NC. Operation and performance of a mass-selective cryogenic linear ion trap. *J. Am. Soc. Mass Spectrom.* 2018; *29*: 2115-2124.

Thompson CJ, Aguirre F, Husband J, Metz RB. Photofragment spectroscopy and dynamics of $NiOH^+$ and $NiOH^+(H_2O)$. *J. Phys. Chem. A*. 2000; *104*: 9901-9905.

Thompson CJ, Faherty KP, Stringer KL, Metz RB. Electronic spectroscopy and photodissociation dynamics of Co^{2+}-methanol clusters: $Co^{2+}(CH_3OH)_n$ (n = 4-7). *Phys. Chem. Chem. Phys.* 2005; *7*: 814-818.

Thompson CJ, Husband J, Aguirre F, Metz RB. Photodissociation dynamics of hydrated Ni^{2+} clusters: $Ni^{2+}(H_2O)_n$ (n = 4-7). *J. Phys. Chem. A*. 2000; *104*: 8155-8159.

Tureček F. Benchmarking electronic excitation energies and transitions in peptide radicals. *J. Phys. Chem. A*. 2015; *119*: 10101-10111.

Tureček F. Flying DNA cation radicals in the gas phase: generation and action spectroscopy of canonical and noncanonical nucleobase forms. *J. Phys. Chem. B* 2021; *125*, 7090-7100. https://doi.org/10.1021/acs.jpcb.1c03674

Vdovin A, Slenczka A, Dick B. Electronic spectroscopy of lumiflavin in superfluid helium nanodroplets. *Chem. Phys.* 2013; *422*: 195-203.

Viglino E, Shaffer CJ, Tureček F. UV-VIS action spectroscopy and structures of tyrosine peptide cation radicals in the gas phase. *Angew. Chem. Int. Ed*. 2016; *55*: 7469-7473.

Wang XB, Wang LS. Development of a low-temperature photoelectron spectroscopy instrument using an electrospray ion source and a cryogenically controlled ion trap. *Rev. Sci. Instrum.* 2008; *79*: 073108.

Wee S, O'Hair RAJ, McFadyen WD. Can radical cations of the constituents of nucleic acids be formed in the gas phase using ternary transition metal complexes? *Rapid Commun. Mass Spectrom*. 2005; *19*: 1797−1805.

Wellman SMJ, Jockusch RA. Moving in on the action: an experimental comparison of fluorescence excitation and photodissociation action spectroscopy. *J. Phys. Chem. A*. 2015; *119*: 6333-6338.

Wyer JA, Brøndsted Nielsen S. Absorption by isolated ferric heme nitrosyl cations in vacuo. *Angew. Chem., Int. Ed.* 2012; *124*: 10402−10406.

Xu S, Smith JET, Gozem S, Krylov AI, Weber JM. Electronic spectra of tris(2,2′-bipyridine)-M(II) complex ions in vacuo (M = Fe and Os). *Inorg. Chem*. 2017; *56*: 7029-7037.

Xu S, Smith JET, Weber JM. The electronic spectrum of cryogenic ruthenium-tris-bipyridine dications in vacuo. *J. Chem. Phys.* 2016a; *145*: 024304.

Xu S, Smith JET, Weber JM. UV spectra of tris(2,2′-bipyridine)-M (II) complex ions in vacuo (M = Mn, Fe, Co, Ni, Cu, Zn). *Inorg. Chem.* 2016b; *55*: 11937-11943.

Yao H, Jockusch RA. Fluorescence and electronic action spectroscopy of mass-selected gas-phase fluorescein, 2′,7′-dichlorofluorescein, and 2′,7′-difluorofluorescein ions. *J. Phys. Chem. A* 2013; *117*: 1351-1359.

Zagorec-Marks W, Foreman M, Verlet J, Weber J. Cryogenic ion spectroscopy of the green fluorescent protein chromophore in vacuo. *J Phys Chem Lett*. 2019; *10*: 7817−7822.

Zollinger H. 1987. *Color Chemistry: Syntheses, Properties and Applications of Organic Dyes and Pigments*, VCH Verlagsgesellschaft mbH, Weinheim, Federal Republic of Germany.

How to cite this article: Tureček F. UV-vis spectroscopy of gas-phase ions. *Mass Spec Rev*. 2023;42:206-226. https://doi.org/10.1002/mas.21726